BLU-RAY CYTOMETER

A thesis
submitted in partial fulfilment
of the requirements for the degree
of
Master of Engineering

by
NASER ALBUGAMI

THE UNIVERSITY OF
WAIKATO
Te Whare Wānanga o Waikato

Hamilton, New Zealand

February 2012

Dedicated to my family

Mum, Dad and siblings

ABSTRACT

The flow cytometers are one of the most powerful devices used to measure the properties of individual particles passing through a sensing region. In this thesis, a low cost cytometer using a Blu-ray pickup is analysed and further developed. This includes the characterisation of the existing system and its performance as well as the evaluation of count rate for different flow rates and focuses. Based on that, the best parameters for measurement conditions have been determined. The system was set up for forward scatter as well as for fluorescence, both were to be measured at the same time and it was found that both could be recorded and counted. In addition, it was found that fluorescing particles can give a fluorescent count as well as scatter count and it was noticed that different sizes of non-fluorescent particles can produce scatter count. The count rate for a mixture of fluorescent and non-fluorescent particles was measured. This required the installation of two different amplifiers (for fluorescent and non-fluorescent particles) and building a new LabView program containing two channels.

In a later part of the thesis, the system was improved to progress towards a setup of avalanche photodiode as detector for forward scattering as well as fluorescence. This gives a very good counting accuracy of 90% at speed of 10μl/s. However, this counting accuracy drops to 80% at speed of 1μl/s when mixing fluorescent and non-fluorescent particles. The counting accuracy is the ratio (in percent) of the measured count to the actual one. As a new detection approach, a beam stop was installed in front of the photo detector so scattered laser light from particles was detected instead of a reduction of laser intensity. This part of the project proves Mie theory which states that the the forward scattered light is in the forward direction. To double check this result, a beam pass was installed in front of the photo detector and the calculated percentage of counting accuracy was very close to the one without a beam stop. It was also checked that the system was capable of detection fluorescent particle after the installation of a high bass filter which passes fluorescent wavelength signals (green) and blocks the blue ray signals. Finally, it was found that this system is able to detect small size particles, such as 1μm particles and to distinguish between 1μm and 10μm particles.

ACKNOWLEDGEMENTS

The writer of this thesis would like to thank Associate Professor Rainer Künnemeyer for his help and advice in writing this thesis and in the laser lab. Mr. Andrew L. Clow, the previous investigator, must be thanked for his help and support in the detection and count particles using the existing Blu-ray setup. Finally, Mr. Pawan Kumar, the lab administrator, should be thanked for his help in the lab and his overall support.

CONTENTS

ABSTRACT……..……v

ACKNOWLEDGEMENTS……vii

CONTENTS……...……....ix

LIST OF FIGURES……...xi

LIST OF TABLES……xv

1. INTRODUCTION……...1

2. LITERATURE OF CYTOMETER AND SIGNAL PROCESSING…….....3

2.1 Literature Review of Cytometer 3

2.1.1 Historical Background 3

2.1.2 Applications 3

2.1.3 Main Components and basic operation 5

2.1.4 State of Art in Flow Cytometer 7

2.2 Signal Processing 27

2.2.1 Signal Detection 27

2.2.2 Signal Enhancement 34

2.2.3 The Use of a Threshold 37

3. EXPERIMENTAL SETUP…….39

3.1 Overview 39

3.2 Illumination System 40

3.3 Detection System 42

3.4 Fluidics System 43

3.5 Data Analysis and Computer System 47

3.5.1 Data Acquisition Module (DAQ) 47

3.5.2 LabView Design and Analysis 48

3.5.3 MATLAB Program 52

4. EXPERIMENTAL PROCEDURES AND RESULTS…...…...55

4.1 Counting Accuracy of 20μm Particles with and without a Beam Stop 55

4.1.1 Design 55

4.1.2 Results and Discussion 56

4.2 Counting Accuracy of 20μm Particles with a Beam Pass 57

4.2.1 Design 57

4.2.2 Results and Discussion 58
4.3 Counting Accuracy of 20µ Particles using normal Photodiode and APD 59
4.3.1 Design 59
4.3.2 Results and Discussion 60
4.4 Counting Accuracy Dependence on Focus 61
4.4.1 Design 61
4.4.2 Results and Discussion 62
4.5 Counting Accuracy of a Mixed of Fluorescent and Non-Fluorescent Particles 63
4.5.1 Design 63
4.5.2 Results and Discussion 63
4.6 Counting Accuracy for Fluorescence Particles as Forward Scattering and Fluorescence Detection with and without Filtering 70
4.6.1 Design 70
4.6.2 Results and Discussion 71
4.7 Counting Accuracy of Fluorescence Particles Using APD and Normal Photodiode with and without Filtering 72
4.7.1 Design 72
4.7.2 Results and Discussion 74
4.8 Counting Accuracy of 1µm Particles in Forward Scattering 75
4.8.1 Design 75
4.8.2 Results and Discussion 76
4.9 Differentiation between 1µm and 10µm Particles 76
4.9.1 Design 76
4.9.2 Results and Discussion 77
5. DISCUSSION……...……79
6. CONCLUSION……..……...81
7. APPENDIX……83
Laser Safety[39] 83
8. REFERENCES……..85

LIST OF FIGURES

Figure 1: Cytometer main components[8] 5
Figure 2: A commercial flow Cytometer manufactured by iCyt Eclipse[9] 8
Figure 3: A commercial cell sorter manufactured by Becton Dickinson[10] 9
Figure 4: Schematic diagram of optical pick-up detection mechanism[11] 10
Figure 5: Fluorescent signal detection at spot by PMT detector: an experimental test condition, b fluorescent signal[11] 11
Figure 6: Focus error signal by autofocusing control[11] 12
Figure 7: DVD cytometer main Circuit[12] 13
Figure 8: Image of the fabricated device (9 mm x 13 mm): 1) sheath inlet, 2) side inlets, 3) sample inlet, 4) detection region, 5) outlet[12] 14
Figure 9: Flow cell for sample injection showing sheath liquid from back and side squeezes the sample closely over the mirror[12]. 14
Figure 10: Sensor readings for erythrocytes (left) and polystyrene counting beads (right). The beads cause an intensity drop while erythrocytes cause a signal rise[12] 14
Figure 11: Histogram for the measurements from Figure 10[12]. 15
Figure 12: DVD Flow cytometer main circuit[13] 16
Figure 13: Measurement principle for determination of dimensions of a microfluidic device[13] 16
Figure 14: FE Signal and corresponding dimensions for the measurement explained in Figure 13[13] 17
Figure 15: Illustration of the main components of a DVD pickup (only the main and 1st order diffracted beams are shown)[14]. 18
Figure 16: The first fabricated flow cell[14]. 19
Figure 17: Photodiode pulse caused by 100µm beads [14]. 20
Figure 18: Photodiode pulse caused by 10µm beads. (a) 1ml/min (b) 10ml/min[14]. 20
Figure 19: Photodiode pulse caused by 3µm beads. (a) Pulses from a single 3µm bead travelling in the x direction (b & c) single pulses from 3µm beads with flow direction along the y-axis. An enlargement of figure (c) is shown inset[14]. 21
Figure 20: 10µm beads taken through dark field microscope. The gold film is visible on the left half of the photo[14]. 21
Figure 21: 3µm beads in flow cell one. On the left is a standard image; on the right is a dark-field image[14]. 22
Figure 22: DVD Optical Pickup Head Setup[16] 23
Figure 23:: PHR-803T Pickup and Dismantled View[17] 24
Figure 24: SF-BD413P Blu-ray Optical Pickup mounted on a sled 25
Figure 25: Size Comparison[20] 27
Figure 26: Forward Scatter Histogram[22] 28
Figure 27: Rayleigh Scattering[24] 28
Figure 28: Mie Scattering for Small (left) and Large (right) Particles[24] 29
Figure 29: 2D Scatter Plot of Blood[26] 30
Figure 30: Energy State Diagram for Fluorescence[27] 31
Figure 31: Two Colour Experiment (Excitation)[29] 32
Figure 32: Two Colour Experiment (Emission)[29] 33
Figure 33: Two Colour Dot Plot[30] 33
Figure 34: Different types of optical filters[31] 34
Figure 35: A picture taken without a contrast method[33] 35

Figure 36: A picture taken with phase contrast method[33] 35
Figure 37: Threshold Level[20] 38
Figure 38: Blu-ray cytometer main setup diagram 39
Figure 39: Laser diode driver 40
Figure 40: Laser Diode in the Blu-ray Pickup 41
Figure 41: PCB Interface Board Circuit Layout[35] 42
Figure 42: The Photo Detector 42
Figure 43: Pre-amplifier 43
Figure 44: Old Pump System 43
Figure 45: New Pump System Components 45
Figure 46: Control Panel for Valve Manifold. 46
Figure 47: Control Panel for Syringe Pump. 46
Figure 48: Topas Chip 4 Parallel Flow Cells 47
Figure 49: The data acquisition module (DAQ) 48
Figure 50: LabView program calculating the set point 49
Figure 51: LabView Program for Automatic Counting (true case) 50
Figure 52: LabView Program for Automatic Counting (false case) 51
Figure 53: LabView Program for creating two channels in Lab view 51
Figure 54: the data obtained from LabView in Excel Sheet 52
Figure 55: A Picture of the Main Circuit for Counting 20µm Particles Using a Beam Stop 55
Figure 56: A diagram of the Main Circuit for Counting 20µm Particles Using a Beam Stop 55
Figure 57: A Beam Stop 56
Figure 58: Percentage of Counting Accuracy of 20µm Particles with and without a Beam Stop 56
Figure 59: A Picture of the Main Circuit for Counting 20µm Particles Using a Beam Pass 57
Figure 60: A diagram of the Main Circuit for Counting 20µm Particles Using a Beam Pass 57
Figure 61: Percentage of Counting Accuracy of 20µm Particles with a Beam Pass 58
Figure 62: A Picture of the Main Setup for Forward Scattering using APD 59
Figure 63: A diagram of the Main Setup for Forward Scattering using Normal Photodiode and APD 59
Figure 64: Percentage of Counting Accuracy of 20µm Particles using normal Photodiode and APD 60
Figure 65: Particle detection for difference laser focus, particles flow perpendicular to the paper 61
Figure 66: Percentage of Counting Accuracy of 20µm Particles for Two Different Focuses 62
Figure 67: Percentage of Counting Accuracy of 10µm Particles 65
Figure 68: Percentage of Counting Accuracy of Fluorescent Particles 67
Figure 69: Percentage of Counting Accuracy of a Mix of 10µm Fluorescing and Non-Fluorescing Particles 68
Figure 70: A picture of the Main Circuit for Forward Scattering and Fluorescence Detection with and without Filtering 70
Figure 71: A diagram of the Main Circuit for Forward Scattering and Fluorescence Detection with and without Filtering 71

Figure 72: Percentage of Counting Accuracy for Fluorescent Particles as Forward Scattering and as Fluorescence Detection with and without Filtering 71
Figure 73: A picture of the Main Setup for APD Fluorescence Detection 72
Figure 74: A diagram of the Main Setup for APD Fluorescence Detection 73
Figure 75: Percentage of Counting Accuracy of Fluorescent Particles Using APD and Normal Photodiode with and without Filtering 74
Figure 76: Percentage of Counting Accuracy of 1µm Particles..... 76
Figure 77: The cytometric outputs for a mix of 1µm and 10µm Particles. 77

LIST OF TABLES

Table 1: The main differences between DVD, HD DVD and Blu-ray 25
Table 2: Blu-ray Laser Mounting Board Pinout. Pin 1 is located closest to the ribbon cable connector on the optical pickup unit..... 41
Table 3: Pump Rates for 10ml Syringe..... 44
Table 4: Experimental Calculations for Counting Accuracy of 10µm Particles..... 65
Table 5: Experimental Calculations for Counting Accuracy of Fluorescent 9.9µm Particles..... 67
Table 6: Experimental Calculations for Counting Accuracy of a Mix of 10µm Fluorescing and Non-Fluorescing Particles..... 69

1. INTRODUCTION

A flow cytometer is an instrument that measures the properties of microscopic particles as they flow in a single file through a sensing region. These instruments are relatively big and expensive, so the aim of this project is to design a system using a Blu-ray optical pickup head which can be developed into a palm held device at a much cheaper price. The optical detection system of a flow cytometer comprises of five main parts: a micro flow channel, a light source, a detector, a signal amplifier and a computer for data acquisition. Many different light sources can be used for particle detection but the two most commonly used ones are lamps and lasers. When the stained cell is passed under the laser beam through a micro flow channel, the cells will get excited and fluoresces. The fluorescent light can be detected and processed electronically to characterise a particular cell, and the information can then be used to electro statically separate cells into sub-populations according to certain desired characteristics.

There are two main disadvantages of commercial cytometers; they are expensive and bulky. They are expensive because they have expensive lasers which have excellent beam quality. This beam is used to create a very small focused spot on each particle as it passes through the region of interaction. Commercial flow cytometers require photomultiplier tubes (PMTs), which are extremely sensitive detectors of light and have a very high gain (as high as 10^6). According to Howard Shapiro, the best efficiency PMTs are too expensive[6]. Commercial cytometers use bulky optical elements such as lenses and spatial filters to achieve small spot size but they create other problems in the beam alignment.

In this thesis, a Blu-ray cytometer is used as a cheap option since some pickups can be bought for only NZ$15. This is quite cheap considering the amount of optics inside these pickup units. The advantage of using Blu-ray, HD-DVD, DVD or CD pickup units is not only the low cost but also the ability to use the integrated magnetic actuators to adjust for alignment errors between flow channel and the pickup which contains low-cost precision optics. Another reason is that the blue laser which is of 405nm wavelength can be focused into a much smaller spot size (as small as 0.5μm).

In the second chapter, the literature review of cytometer and signal processing is discussed. This includes the main components, which are the state of the art and latest semiconductor diodes in flow cytometers. The third chapter, talks about the experimental setup, main part details and LabView design and analysis. In the fourth and fifth chapters, experimental procedure, results and discussion will be elaborated.

2. LITERATURE OF CYTOMETER AND SIGNAL PROCESSING

2.1 Literature Review of Cytometer

2.1.1 Historical Background

A flow cytometer is an instrument that measures cells or other particles as they flow in single file through a sensing region[2]. The original name for this technology was 'pulse cytophotometry' (In German Language 'Impulszytophotometrie'). The first impedance-based flow cytometer device was invented by Wallace H. Coulter in 1953[3]. The first fluorescence-based flow cytometer device was developed by Wolfgang Göhde in 1968 from the University of Münster and it was manufactured by Partec through Phywe AG in Göttingen in 1969[3]. In 1976, the name of this technology had been changed from 'pulse cytophotometry' to 'Flow Cytometer' at the 5th American Engineering Foundation Conference on Automated Cytology in Florida. Historically, electrical methods were used to count particles but they are not commonly used now. One exception was in 2003, when Huang et al. demonstrated the detection, and the evaluation of the membrane integrity of individual cells in a microfluidic channel using a 50mVrms, 500Hz electrical signal applied to a pair of electrodes[4]. Another example was in 2006, when Cho et al. developed a device for measuring the electrical contact resistance for individual red blood cells using twin microscale cantilevers[5].

2.1.2 Applications

There are many applications for flow cytometers including immunophenotyping (a cell identification technique) and ploidy analysis (the number of sets of chromosomes in a biological cell). Flow cytometers can be used for green fluorescent protein (GFP) expression analysis (a fluorescent marker frequently used in molecular biology and neuroscience). Other uses include, cell counting, molecular biology, pathology, immunology, plant biology and marine biology. The following are some applications discussed briefly.

Protein Engineering

In protein engineering, flow cytometers are used after the synchronisation with yeast display and bacterial display (a technique used for in vitro protein evolution)

to determine cell surface-displayed protein variants with required features[2]. Rational design and directed evolution are two main strategies in protein engineering. These two strategies are used together for cell identification in flow cytometer.

Food Industry

In food microbiology, food-borne pathogens can be detected by the help of flow cytometer. Flow cytometer can be used to classify and characterise food bacteria, like Escherchia. Furthermore, flow cytometer can be used to count somatic (nucleated) cells in milk in order to examine the health status of a cow's udder and to make sure that its milk is suitable for human consumption[6].

Medicine

In medicine, a flow cytometer is used in transplantation, hematology, tumour immunology and chemotherapy, prenatal diagnosis, genetics and sperm sorting for sex preselection[3]. Flow cytometer can also be used as cell-to-cell communication in the tumour promoters' process.

Marine Biology

In marine biology, particles concentration, community structures, abundances and the autofluorescent properties of photosynthetic plankton for aquatic organisms can be studied and characterised using flow cytometers. In addition, marine dinoflagellate *Gonyaulax* which causes 'red tide' can be determined using flow cytometers[3].

DNA Analysis

The haploid set of the chromosomes in the human genome can be mapped using flow cytometers. To elaborate this, the base sequence of every gene in the human genome can be identified, their locations mapped and a DNA library is produced. In addition, flow cytometers can help to determine the accuracy of DNA distribution analysis[7].

2.1.3 Main Components and basic operation

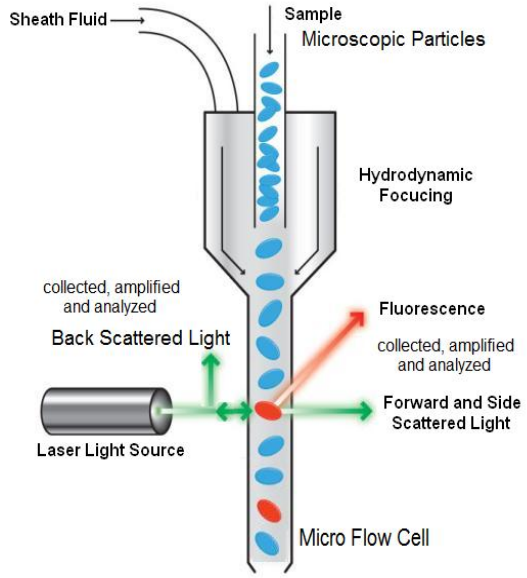

Figure 1: Cytometer main components[8]

A flow cytometer consists of the following five main components as shown in Figure 1:

- A fluidic system including a micro flow cell, which presents samples to the interrogation point and takes away the waste.
- The laser system which is the light source for scatter and fluorescence.
- The optics, which gather and direct the light.
- The detectors, which receive the light.
- The electronics and the peripheral computer systems, which convert the signals from the detectors into digital data and perform the necessary analysis.

Basic Operation

The flow cytometer analyses the particles by passing thousands of cells per second through a laser beam and detects the light that hits each cell and then analyses three types of detected signals: backward scattering, forward scattering and florescent emission. After that, the gathered information can be analysed statistically by a flow cytometer software program to obtain some characteristics such as size, complexity, phenotype and health.

The Interrogation Point

The interrogation point is the heart of the system. This is where the laser and the sample intersect and the optics collect the resulting scattered and fluorescent signals. To get accurate data collection, it is important that particles or cells are passed through the laser beam one at a time. Most flow cytometers accomplish this by injecting the sample stream containing the cells into a flowing stream of sheath fluid using hydrodynamic focusing where the sample stream becomes compressed to roughly one cell in diameter[7].

Laser System

As a cell passes through the laser, it refracts or scatters light at all angles (Rayleigh and Mie scattering). Forward scatter, or low-angle light scatter, is the amount of light scattered in the forward direction as laser light strikes the cell. The magnitude of forward scatter is roughly proportional to the size of the cell, and this data can be used to quantify that parameter[6]. If fluorescent molecules such as fluorophore-labelled antibodies are used, fluorescent signals will be generated when laser with a suitable wavelength hits a particle. This happens when a fluorophore gets excited to a higher energy level followed by the return of that fluorophore to its ground state with the emission of light.

Photo Detector and Beam Stop Bar

The scattered light from the laser light is quantified by a detector that converts intensity into voltage. A detector which incorporates gain is required for weak signals (usually fluorescent signals) otherwise the amplifier noise will be too high compared to the signal. Photomultiplier tubes (PMTs) and avalanche photodiodes (APD's) are the two main types of detectors used in flow cytometers. The PMTs are extremely sensitive detectors of light and have a very high gain (as high as 10^6) while APD's have a gain from 40 to 100 and have more noise.

In most cytometers, a beam stop bar (called an obscuration bar) is placed in front of the forward scatter detector. The obscuration bar prevents any of the intense laser light from reaching the detector. As a cell crosses the laser, light is scattered around the obscuration bar and is collected by the detector[2].

2.1.4 State of Art in Flow Cytometer

2.1.4.1 Cytometer in the Market

Many companies have manufactured flow cytometers for the last 50 years but now only a few of them are in business. High performance commercial cytometers have many features over the low cost cytometers but they are very expensive. To illustrate that, whereas the low cost approach cytometer may cost US$200, the commercial flow cytometers may cost US$50,000.

Flow cytometers may cost three to five times the cost of parts inside them due to their expensive parts, such as lasers and PMT's. It is possible to find a two-beam cell sorter cheaper than one with a single- beam analyser. However, it may be better to buy the expensive one if its manufacturer has a good reputation and better support after sale, particularly if the flow cytometers need to be used for a medical application, like curing cancer[6].

All types of flow cytometers are able to analyse several thousand particles per second. Some are also able to separate and isolate the microscopic particles depending on their properties. Moreover, they draw on a number of physical disciplines including fluidics, optics, analogue and digital electronics, and data acquisition. Several properties of each cell, such as size, structure and internal cellular content can be detected as the cells pass through the flow cell. Particles as small as 0.1μm are detectable and the accuracy of measurement of commercial cytometers can reach the precision of a few percent at analysis rates of thousands of cells per second.

There are many different types of flow cytometers available in the market and they have different sizes and prices. The prices normally depend on the size of the device the smaller and more compact, the more expensive. It was found that the price for flow cytometers ranges from approximately US$15,000 to US$100,000 or even more and there are many different companies involved in developing this device.

It should be noted that many flow cytometers do not even deal with analytical cytology. So, it is necessary to know that there are two main types of these instruments: flow cytometers and cell sorters. Whereas flow cytometers are able

to measure the properties of individual particles, cell sorters have the same features as flow cytometers but they can also remove selective objects from the liquid suspension. Figure 2 shows a flow cytometer manufactured by iCyt Eclipse and it has the following features:

- 5-colours, forward scatter, side scatter and cell volume (size).
- Accurate sizing by electronic volume measurement.
- Accurate absolute cell count with high precision syringe delivery mechanism.
- High throughput sample loader:
  - Automated sample preparation.
  - Sample staining and suspension.
  - For both tube and multi-well plate formats.
- Software including database management.
- 24-bit data acquisition with up to six decade logarithmic scale display.

Figure 2: A commercial flow Cytometer manufactured by iCyt Eclipse[9]

Figure 3 shows a cell sorter manufactured by Becton Dickinson and it has the following features:

- Three water-cooled lasers, 488nm, 385nm, and a variable wavelength laser (685nm).

- Seven detector photomultipliers, FSC, SSC, FL1-FL5.
- 50, 70, 100, 200, 300, 400µm nozzle tips.
- Four way sort assembly with cooling.
- Turbo sort high pressure option.
- Clone Cyt option.
- HP XXX workstation with dual Xeon 1.7GHz and 2GB RAM.

Figure 3: A commercial cell sorter manufactured by Becton Dickinson[10]

2.1.4.2 Low Cost Cytometers

As it was mentioned in the previous section (2.1.4.1), commercial flow cytometers are expensive. This leads researchers to think of alternative options of cheap flow cytometers, such as low cost cytometers based on DVD technology. In this part, four papers based on DVD technology will be presented. They are "A new DNA chip detection mechanism using optical pick-up actuators"[11], "Low Cost Cytometer Based On A DVD Pickup Head"[12], "DVD pickup heads for optical measurement applications"[13] and "Low cost optical particle detection for Lab on Chip systems based on DVD technology"[14].

1) **"A new DNA chip detection mechanism using optical pick-up actuators"**

   In this paper, the authors were able to set up a new optical detection system for DNA-chip using an optical pick-up that uses a commercial DVD pick-up with 650nm laser diode by modifying the optical path. They utilised the

laser beam in the pickup for dynamic auto focusing and exciting fluorescent light of Cy5 dye which is measured by a high sensitive detector. This auto focusing control was done by a voice coil motor actuator which gives high scan speed, low optical distortion and high alignment accuracy. Figure 4 describes the schematic diagram of the authors' circuit.

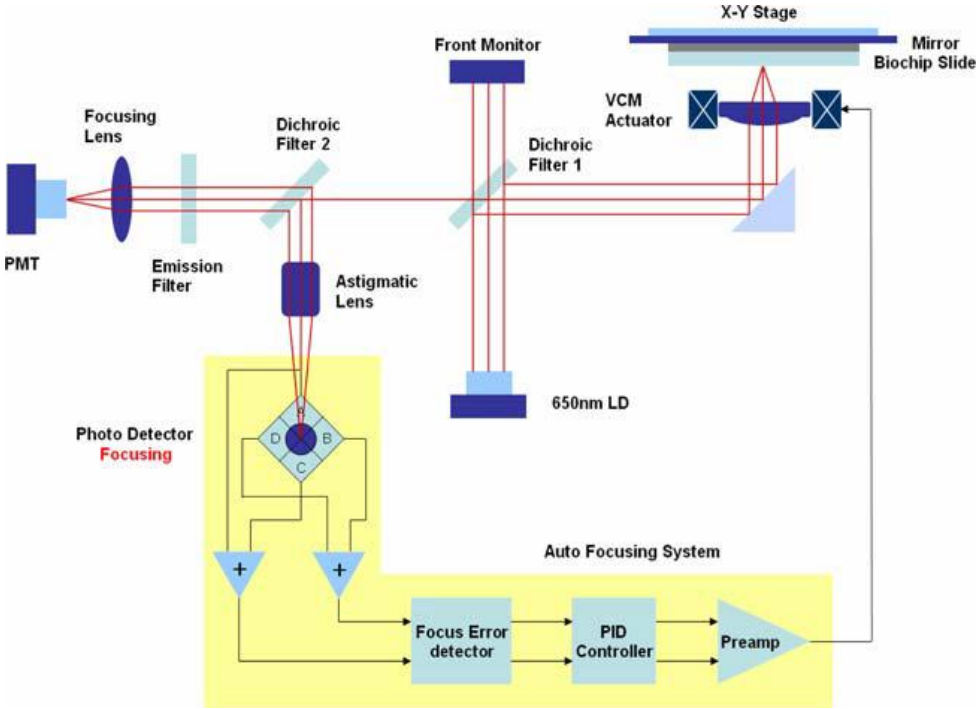

Figure 4: Schematic diagram of optical pick-up detection mechanism[11]

As it can be seen in Figure 4, there are two different optical paths, one is for focusing motion and the other one is for the fluorescence detection. Most of the laser beam, emitted from the laser diode, is reflected by a dichroic filter and the remaining part of the laser beam is used to maintain the laser power constant at the front monitor. After that, it is focused on the reflective layer through the total reflection mirror and objective lens. Next, it is reflected from the reflective layer and the second dichroic filter.

The fluorescent signal will be emitted by the laser beam focused by objective lens and the collimated emission beam is then refocused by detection lens, and passes through a pinhole into the PMT. Figure 5 shows the fluorescent signal detection at spot by PMT detector.

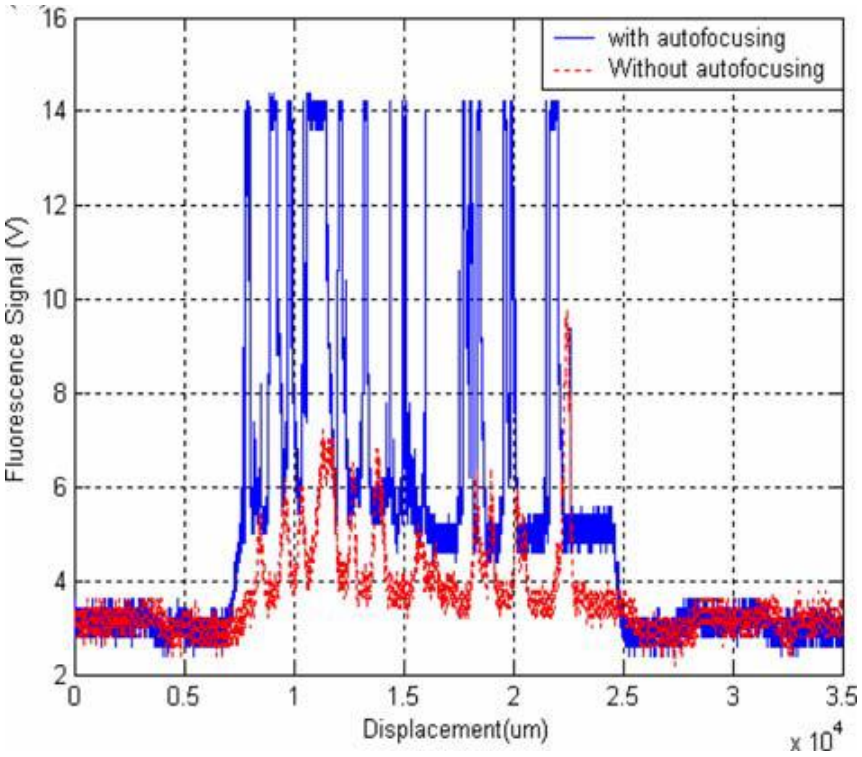

Figure 5: Fluorescent signal detection at spot by PMT detector: an experimental test condition, b fluorescent signal[11]

It can be seen from Figure 5 that the output voltage level by PMT shows the intensity of fluorescent light and it is almost constant regardless of the displacement for the signal without auto focusing. This proves that the dynamic auto focusing mechanism can improve the detection performance. However, the elevation of SNR is due to the uniform background by dynamic auto focusing, the increase of fluorescent signal by the reflective layer and the decrease of noise. Figure 5 also shows that the detection level is almost two times greater than that at the non-focusing state. This is because of the background noise and focus error signal. So, this new circuit shows that the auto focusing mechanism using the DVD optical pick-up improves the detection performance compared to conventional DNA-chip scanners using the single point method.

The authors used equation (1) to calculate the focus error signal:

$$FES = (A + C) - (B + D) \quad (1)$$

Where A, B, C and D are the intensities of four divided regions of the photo detector.

If FES = 0, it means that the lens focus is at perfect focus and if FES > 0, it means that the objective is located closer than the target position. Finally, if FES < 0, this means that the objective is far away. This signal is used to move the VCM actuator. Figure 6 shows the focus error signal by auto focusing control.

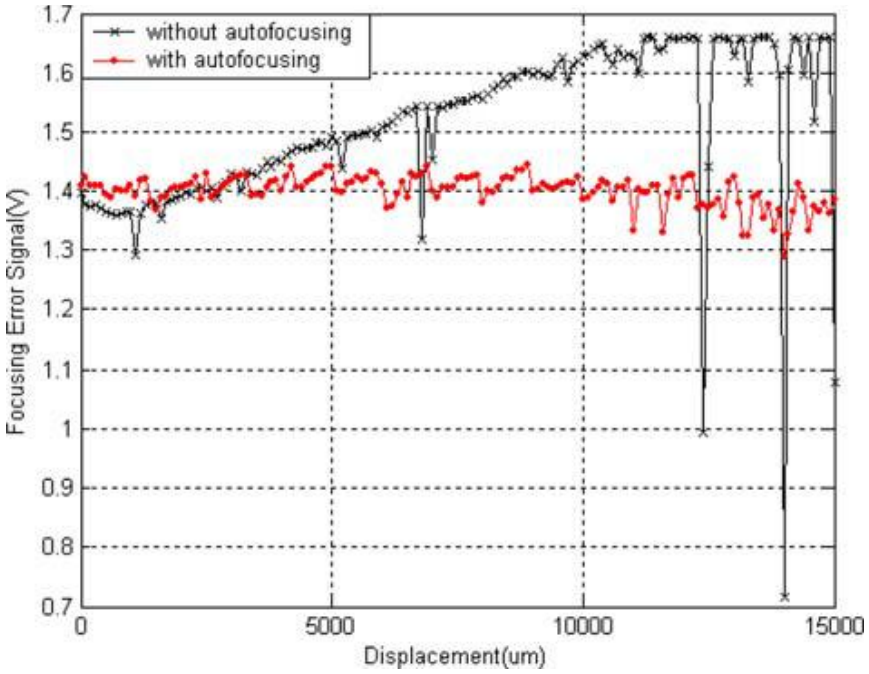

Figure 6: Focus error signal by autofocusing control[11]

As it can be seen from Figure 6, the focusing error signal is almost constant regardless of the displacement of the auto focused signal. However, the other curve indicates the mixed signal includes reflection light from the reflective layer attached on the DNA-chip. In this case, focusing error signal increases for high displacement and this is because of the background noise, surface variability and misaligned chip.

So, the reflective layer improves the reflection ratio and the new detection system, by using a reflective layer attached on DNA chip, is better than the conventional one. This is because it has the following advantages: the use of the existing DNA chip slide, the improvement of focusing readback signal by increasing the reflection ratio and high SNR by increasing the collection efficiency.

2) "Low Cost Cytometer Based On A DVD Pickup Head"

In this paper, the authors were successful in using a DVD pickup system to distinguish between erythrocytes and polystyrene counting beads in a two parameter histogram. Figure 7 shows the system they used to show the cytometric separation of erythrocytes from polystyrene counting beads.

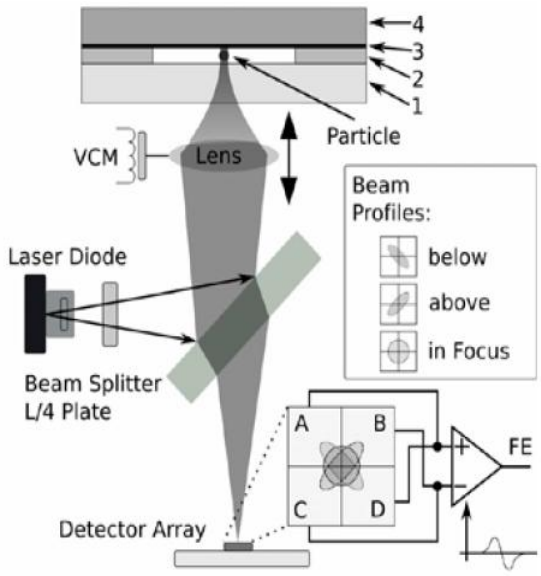

Figure 7: DVD cytometer main Circuit[12]

From Figure 7, the 650nm laser beam is generated from the laser diode, it goes through the beam splitter and then it is focused to a small spot on a reflective surface inside a microchannel. After that, it reflects and goes back to the beam splitter again and propagates towards a four quadrant photodiode array which measures the reflected intensity. The voice coil motor (VCM) is used to control the lens position. If the beam is reflected at its focal point, the beam profile at the detector becomes circular. If the beam is not reflected at its focal point, an astigmatic distortion causes the profile to be elliptic with the principal axis depending on the sign of the focus error (FE). An electric signal proportional to FE is calculated by adding: A+D-B-C (as in equation 1 but with exchanging C and D).

It is difficult to control the position at which the beam hits the particle because of the small focal spot caused by the high numerical aperture of the beam (NA=0.6). This is why the authors use the designed flow cell in Figure 8.

Figure 8: Image of the fabricated device (9 mm x 13 mm): 1) sheath inlet, 2) side inlets, 3) sample inlet, 4) detection region, 5) outlet[12]

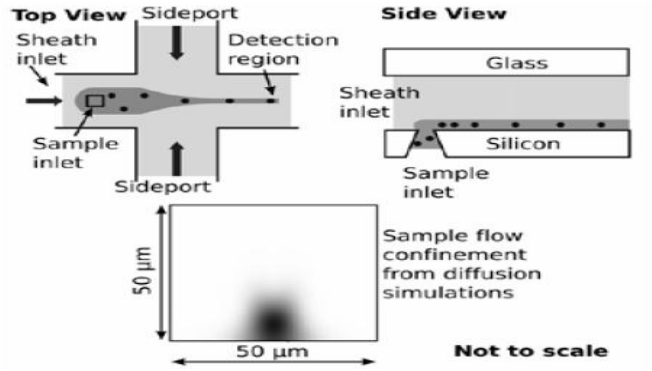

Figure 9: Flow cell for sample injection showing sheath liquid from back and side squeezes the sample closely over the mirror[12].

In Figure 9, the new fabricated flow cell is shown; it was designed to have a precise positioning of the sample flow in the detection region. The purpose of the sheath liquid from the back and side is to squeeze the sample flow to a close distance to the reflective surface using syringe pumps. Figure 10 and Figure 11 show the results obtained from the experiment.

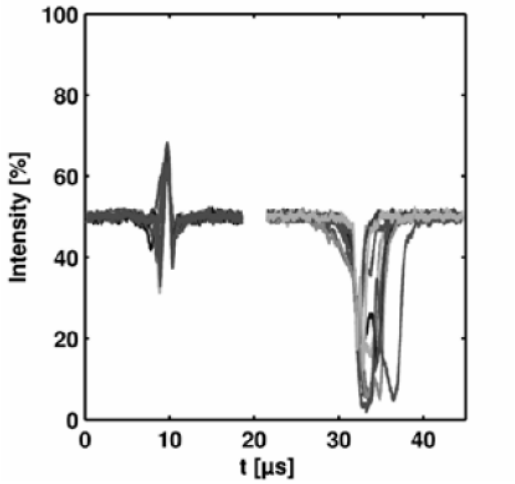

Figure 10: Sensor readings for erythrocytes (left) and polystyrene counting beads (right). The beads cause an intensity drop while erythrocytes cause a signal rise[12].

Figure 10 shows the sensor readings for erythrocytes (left) and polystyrene counting beads (right). It can be seen clearly that the current system was able to distinguish between two types of particles; the beads cause an intensity drop while erythrocytes cause a signal rise.

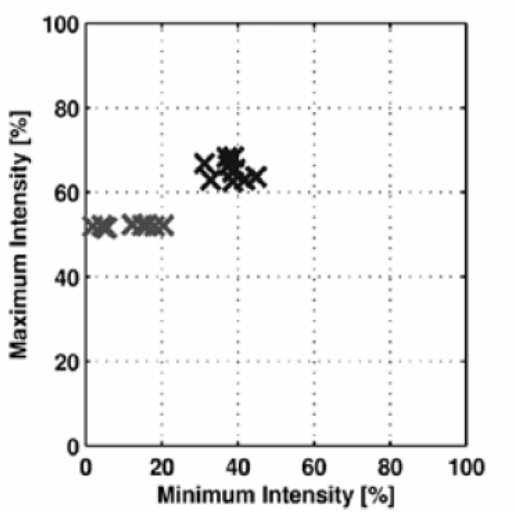

Figure 11: Histogram for the measurements from Figure 10[12].

Figure 11 shows the histogram of the measurements. The signs to the left represent erythrocytes beads and the signs to the right represent polystyrene counting beads. Therefore the plot clearly shows two sub-populations in the sample.

3) "DVD pickup heads for optical measurement applications"

In this paper, the authors were able to use a DVD pickup as a high precision optical measurement system of channel depths (in the range of 20µm to 1000µm) and for detection of flowing cells. This was done by using the optical stylus probe for measuring dimensions of microchannels. The new system can work for all regions even for those that were mechanically not accessible (e.g. covered by a glass lid) if the light can pass through. On the other hand, the current optical measurement system is complicated, it has a complex structure, needs calibration and cannot measure the regions covered by a glass lid. As a result of this, they are expensive and can be used only for high cost applications. The second advantage of the new system is that it is relatively cheap compared to the

existing conventional systems since it uses a DVD pickup. The authors used the setup in Figure 12 for their project.

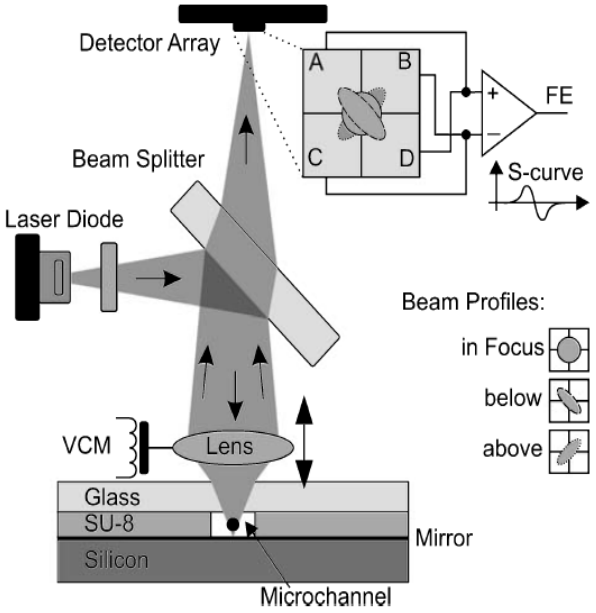

Figure 12: DVD Flow cytometer main circuit[13]

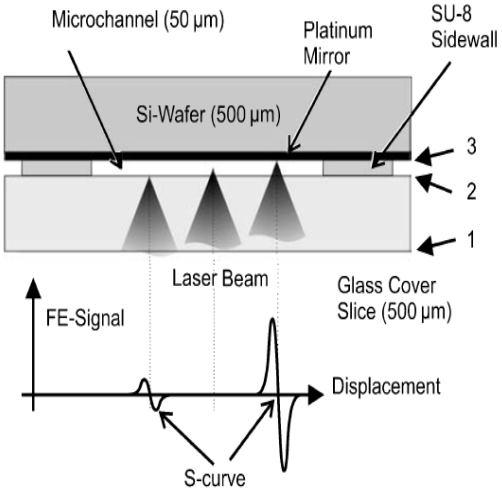

Figure 13: Measurement principle for determination of dimensions of a microfluidic device[13]

The general process of this system (Figure 12) has been explained in paper 2 “Low Cost Cytometer Based On A DVD Pickup Head”. However, the focus in this project is in the microchannel side (Figure 13) which will be explained in detail in this part in order to elaborate how to use this circuit as a laser scanner for determination of the dimensions of a microfluidic

device. In normal operation, the system is kept in focus and the scanning is along a plane. However, in this case the focus actuator is used to scan perpendicular to the focus plane using a VCM. The optical stylus probe moves up and down to adjust the focal point. Every time the focal point hits the (semi) transparent area (between 1 and 3 in Figure 13) a corresponding FE signal is generated. The amplitude of the generated signal depends on reflectivity of this area (between 1 and 3 in Figure 13). Each time the beam passes a reflective surface, there will be a zero crossing (S-curve) in the FE. To make a difference in time between different zero crossings proportional to the distance between the areas, the VCM moves with constant speed. If the focus point lies inside any involved material, a correction factor must be considered because the light propagation speed depends on the refractive index of this material. Therefore, when the time difference is measured, the distance can also be measured. Figure 14 shows the FE Signal and corresponding dimensions for the measurement explained in Figure 13.

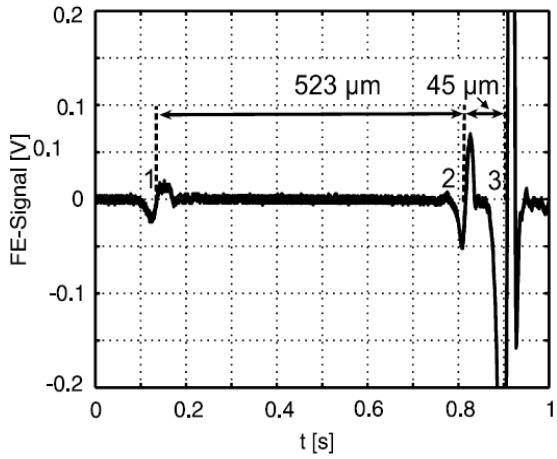

Figure 14: FE Signal and corresponding dimensions for the measurement explained in Figure 13[13].

Figure 14 shows FE Signal and the corresponding dimensions for the measurement explained in Figure 13. Numbers 1, 2 and 3 in Figure 14 represent locations at each crossing which correspond to the areas described in Figure 13. The distance between 1 and 2 (523µm) represents the dimension of the glass cover slice and the distance between 2 and 3 (45µm) represents the dimension of the microchannel. However, there are some limitations to the new proposed system. The first drawback is that

this system is not able to detect zero crossing if the two semi-reflective boundaries are too close to each other (like thin films on top of each other). This is because the S-curves caused by the different layers would overlap. The other disadvantage of the new setup is the necessity for material layers to be transparent since the light beam needs to pass through. This system can also be used to measure the thickness of a resist layer before and after a wafer bonding process.

4) **"Low cost optical particle detection for Lab on Chip systems based on DVD technology"**

In the paper, the authors were able to successfully detect polystyrene beads (represented biological cells) down to 3µm in diameter using a DVD pickup. Figure 15 shows the experimental setup in which an optical pickup was removed from a commercial DVD player (G1928, DickSmith Electronics, NZ).

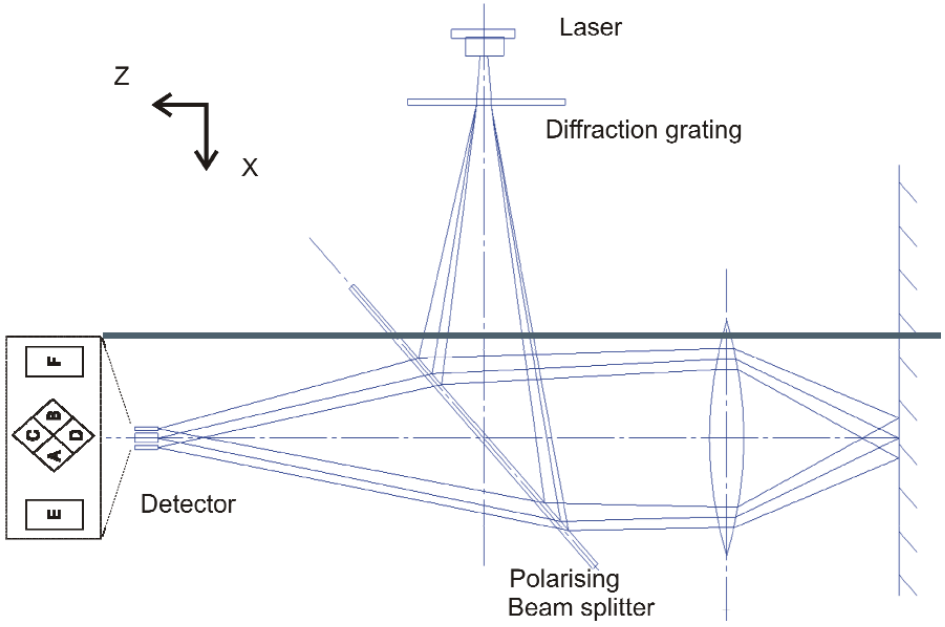

Figure 15: Illustration of the main components of a DVD pickup (only the main and 1st order diffracted beams are shown)[14].

As Figure 15 shows, the diode laser emits a 635-650nm wavelength signal which goes through a diffraction grating. After that, several beams are produced from the diffraction grating and focused by a beam splitter and the main lens onto a target. Then, the light reflected or scattered from the target is collected by the lens and is focused onto a detector array.

There are two electromagnetic coil actuators to focus the lens by translating in the z direction and to shift the focal point in the y axis by tilting the lens about the x axis. These two actuators are also used for autofocus, data retrieval, and tracking. The 0th order beam is detected by A to D detectors and the ± 1st order diffracted beams are detected by the outer detectors E and F.

The authors fabricated electronic circuits to provide current to the laser diode and to adjust the focus of the system. They also fabricated two flow cells for the polystyrene particles; Figure 16 shows the first flow cell.

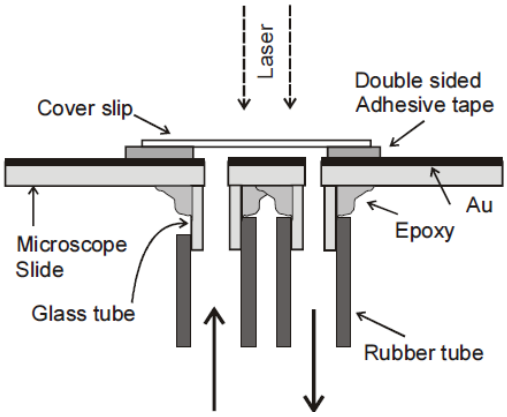

Figure 16: The first fabricated flow cell[14].

The first fabricated cell was used for 3µm and 10µm beads. It was made by using double sided tape as a spacer between a microscope slide and a cover slip. In the microscope slide, the upper surface was coated by 100nm thick gold to create the reflective surface. The polystyrene particles can go from two holes were diamond drilled through the gold coated slide into the microchannel. The dimensions of the first flow cell are 105±10µm thick and 3-4mm width.

However, the second flow cell was used for 100µm beads and it has the same design as the first flow cell but its internal thickness is 300±20µm. This thickness comes from the microscope cover slips which were used as spacer elements between two microscope slides.

The authors also fabricated an aluminium frame for coarse alignment using micrometre screw adjustment. Finally, rubber tubes were used to connect the flow cells to a syringe pump (PHD 2000, Havard Apparatus, Holliston, MA).

Results and discussion

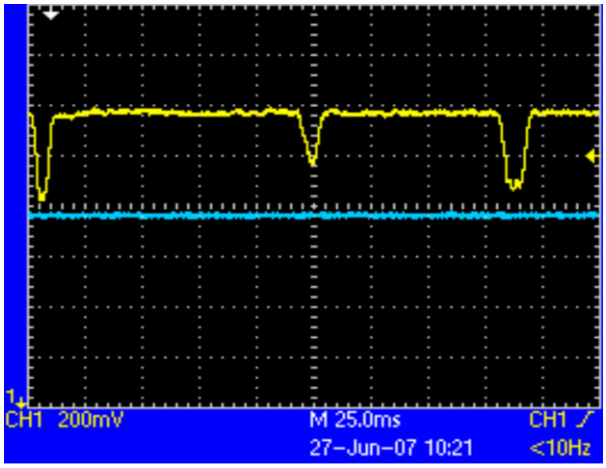

Figure 17: Photodiode pulse caused by 100µm beads [14].

The authors were able to detect 100µm polystyrene beads in the second flow cell as shown in Figure 17 (the lower trace is the baseline signal when no light is received by the photodiode). In Figure 17, three beads were detected and this proves the benefit of using backscattered signals. To elaborate that, a very high reduction in the signal level is generated when the beads enter the measurement volume light. This result also helps to prove the ability of this system to count large biological cells.

The first flow cell was used to detect smaller beads. For example, 10µm beads at water flow rates of 1ml/min and 10ml/min were detected as in Figure 18.

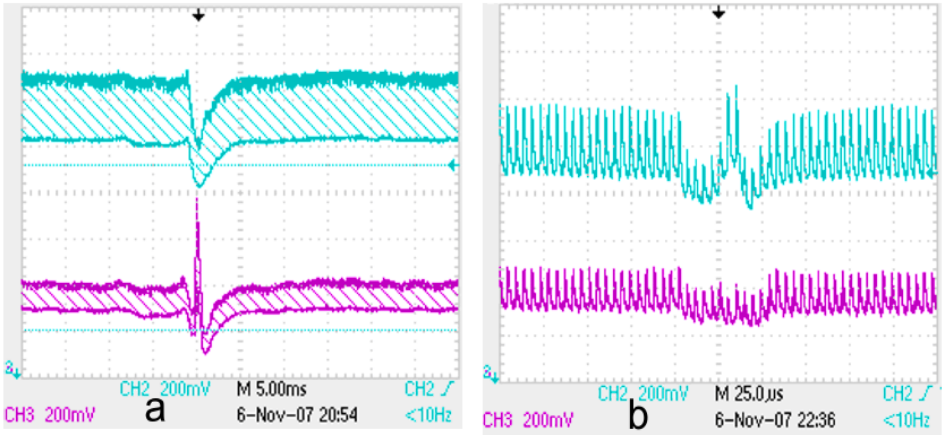

Figure 18: Photodiode pulse caused by 10µm beads. (a) 1ml/min (b) 10ml/min[14].

In Figure 18, the two traces represent the intensity change recorded by the two detectors used in the DVD pickup. In this setup, the laser output was

modulated at 210 kHz which produced a ripple on the photodiode detector voltage (was removed by setting the oscilloscope to the minimum detection peak). Similarly, 3µm polystyrene beads at a water flow rate of 0.007-0.02ml/min were detected in the first flow cell and by the current setup as shown in Figure 19.

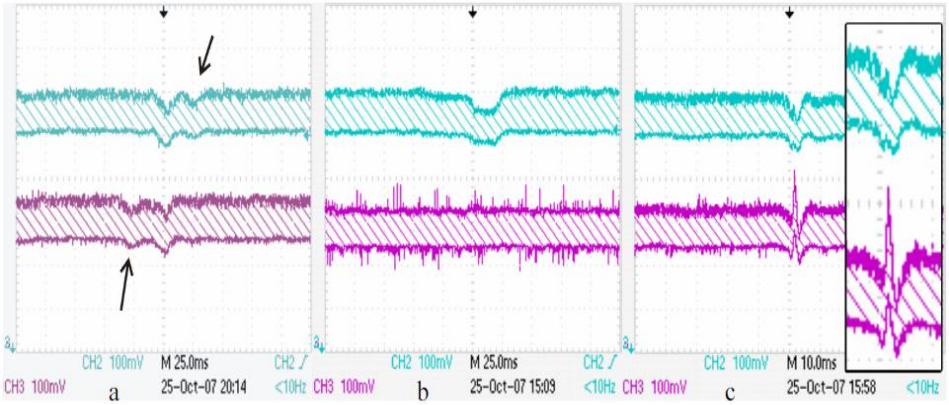

Figure 19: Photodiode pulse caused by 3µm beads. (a) Pulses from a single 3µm bead travelling in the x direction (b & c) single pulses from 3µm beads with flow direction along the y-axis. An enlargement of figure (c) is shown inset[14].

In order to double check that this circuit is able to detect polystyrene beads in the flow channels, the beads were also observed using bright-field and dark-field microscopy. Figure 20 shows the 10µm beads and Figure 21 shows the 3µm beads in the fabricated flow cells. The lines visible in both figures are scratches in the gold film.

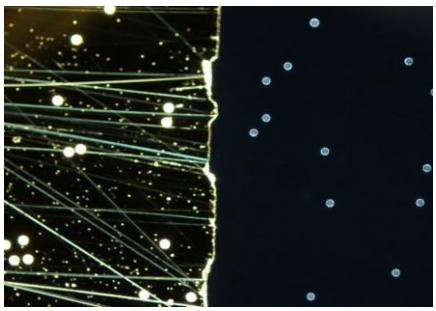

Figure 20: 10µm beads taken through dark field microscope. The gold film is visible on the left half of the photo[14].

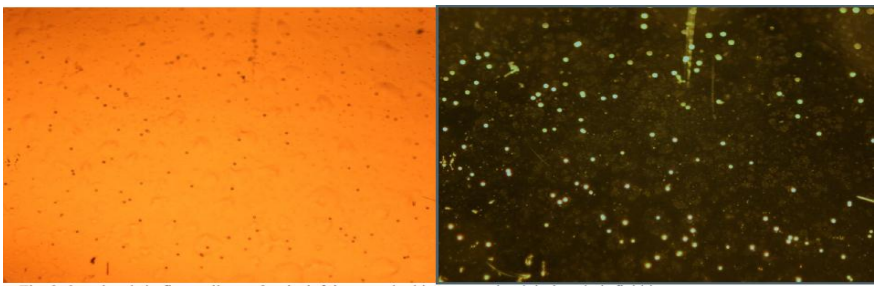

Figure 21: 3µm beads in flow cell one. On the left is a standard image; on the right is a dark-field image[14].

2.1.4.3 DVD, HD DVD and Blu-ray

In this part, DVD (Digital Video Disk), HD DVD (High Definition Digital Video Disk) and Blu-ray technologies will be discussed briefly since they are used in the new low cost approaches for flow cytometers. They are very cheap compared to commercial cytometers (they may cost ~ NZ$15) and this is quite cheap considering the amount of optics inside their pickup units. The advantage of using them is not only their low cost but also the ability to use their integrated actuators which are used to move the laser beam horizontally and vertically to adjust for alignment errors. They have different wavelengths (405nm for Blu-ray & HD DVD and 650nm for DVD) and very small beam focuses (can be focused into a very small spot size, as small as 0.5µm for the Blu-ray discs).

DVD

A DVD (Digital Video Disk) is a flat, circular disc which stores digital data in the form of pits (0's and 1's) and is usually made of aluminium. In 1995, Philips, Sony, Toshiba, and Panasonic invented and developed DVDs which can store more digital data than Compact Discs (CD) even though they are the same size. Whereas CD discs use 780nm wavelength (infrared), DVD discs use 650nm wavelength (red laser)[15]. Figure 22 explains how DVDs work.

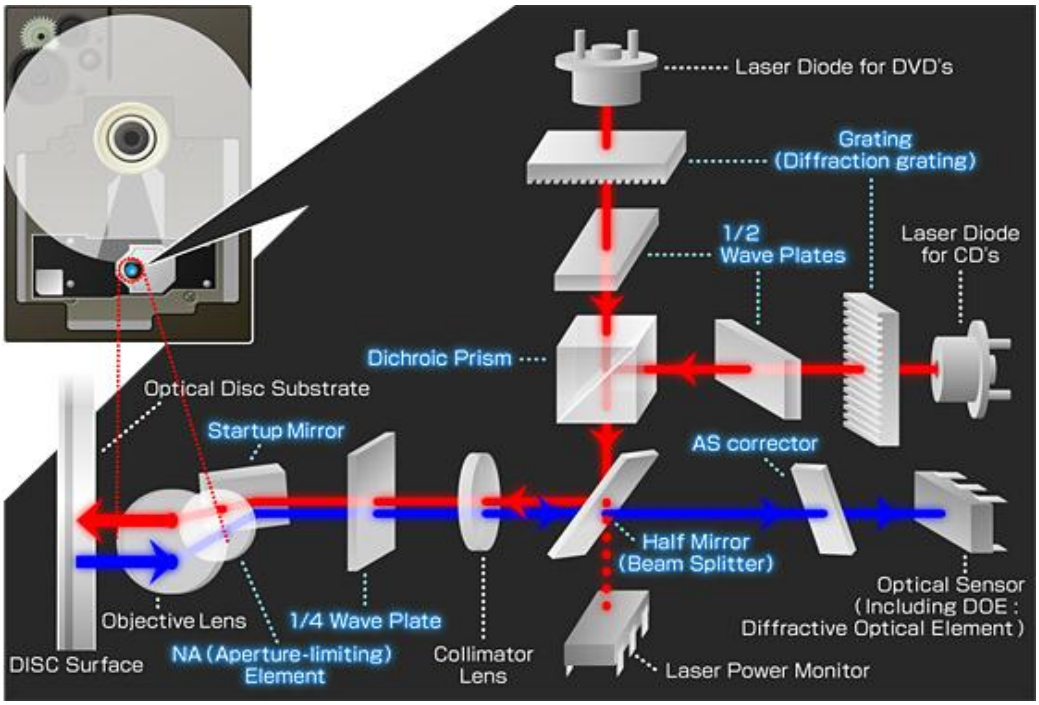

Figure 22: DVD Optical Pickup Head Setup[16]

As shown in Figure 22, a DVD pickup head consists of different wavelength laser beams to be used on Compact Disk (CD) and Digital Video Disk (DVD). First, the laser beams are emitted from the internal laser diodes. After that, it goes through diffraction grating which is used to produce several beams from a single laser beam. These beams then go through ½ wave plate, a series of mirrors and a beam splitter. After that, they are projected to a reflective surface (e.g. data layer on a DVD). Next, the beams return back into the optical head and the reflected beams are processed and converted into an automatic focus error detection signal, automatic tracking error detection signal and information data (an electrical signal). When a focus error signal and a tracking error signal are detected from the reflected beams, focus and tracking adjustments of the coils are performed automatically.

HD DVD

A HD DVD (High Definition Digital Video Disk) optical pickup works in the same way as a normal DVD player except that it has an extra violet laser beam for high definition disks (405nm wavelength). It contains coherent laser beam sources, a grating, a polarising beam splitter, a ¼ wave plate, solid-state detectors, a range of a focus error signal is ±1μm and range of a tracking error signal is ±0.1μm. Figure 23 shows a typical HD DVD[16].

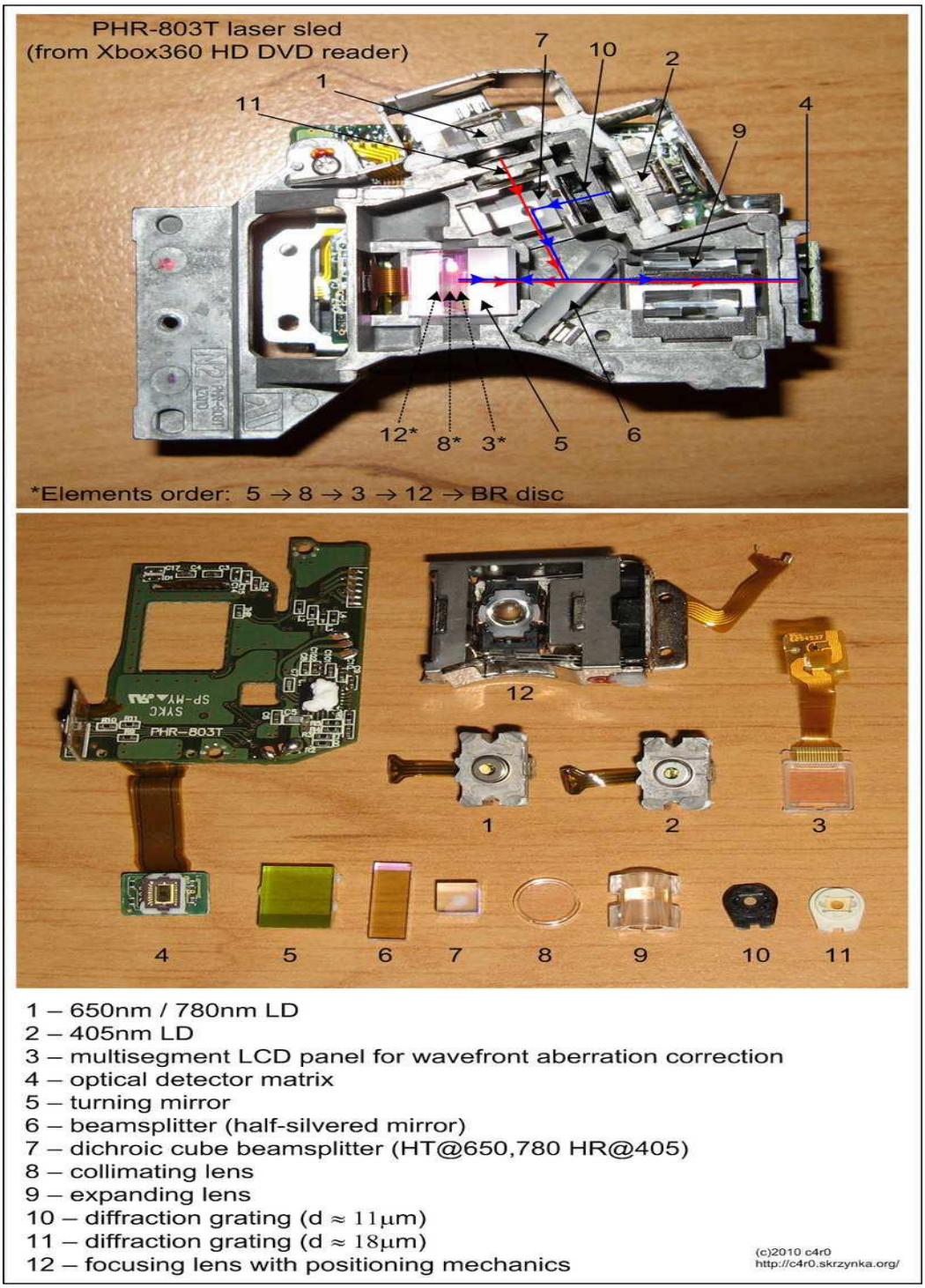

Figure 23: PHR-803T Pickup and Dismantled View[17]

The HD DVD pickup head consists of three different wavelength laser beams to be used on a Compact Disk (CD), a Digital Video Disk (DVD) and a Blu-ray Disk or a HD DVD depending on the disk used. A laser beam passes through a beam splitter and is projected to a reflective surface (e.g. data layer on a DVD) and then propagates to a photodiode detector array.

Blu-ray

The Blu-ray has the same wavelength as HD DVD (405nm); this is a shorter wavelength than a red laser (650nm) which allows data to be packed more tightly and stored in less space. However, HD DVD has almost the same numerical aperture as DVD (for HD DVD, NA=0.65 and for DVD, NA=0.6) while a Blu-ray pickup has a numerical aperture of 0.85. This is what enables Blu-ray Discs to store more data than HD DVD (25GB/50GB for Blu-ray and 15GB/30GB for HD DVD) and to have smaller laser spot sizes with even greater precision (0.62 micron for HD DVD and 0.48 micron for Blu-ray). On Tuesday, 28 March 2008, Toshiba officially announced that they would stop producing HD DVD products and ended the two-year war between HD DVD and Blu-ray18. Figure 24 shows a SF-BD413P Blu-ray Optical Pickup mounted on a sled and Table elaborates the main differences between DVD, HD DVD and Blu-ray.

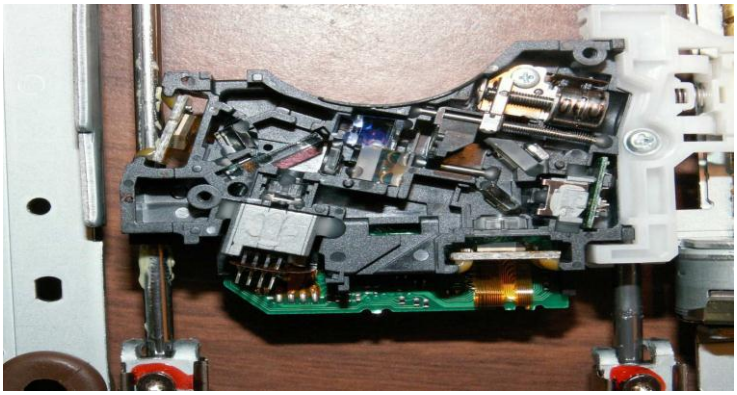

Figure 24: SF-BD413P Blu-ray Optical Pickup mounted on a sled

Table 1: The main differences between DVD, HD DVD and Blu-ray

	DVD	**HD-DVD**	**Blu-ray**
Wavelength	650nm	405nm	405nm
NA	0.6	0.65	0.85
Spot Size	1.1 micron	0.62 micron	0.48 micron
Transparent Protective Layer (Cover Layer)	0.6mm	0.6mm	0.1mm
Capacity(SL)	4.7GB	20GB	25GB
Transfer rate	11.08Mbps	36Mbps	36Mbps

(SL) = Single Layer**, (NA) =** Numerical Aperture

2.1.5 Latest Semiconductor Diodes in Cytometry

In the previous sections, it was mentioned that cytometers in the market are expensive and do not use a low cost approach. However, this situation is to be changed soon since Sony, the global electronics giant, has started working in this field and is developing a new type of a low cost approach[19]. Osamu Kumagai, Senior Vice President of Sony Corporation says Sony is working on ways to combine the use of laser diodes and optical pick-up technology, used in CD and DVD players, to develop a device that could detect the exact location of biomolecules and targeted cells. "We can bring this kind of technology into the medical area. It is a big challenge for us," says Kumagai.

He stated that Sony's flow-cytometer technology will play a big part in the medical field in the future. For example, Sony's devices will be able to detect one cell in a million particles.

Regarding Sony's research in laser diode, they are developing a laser diode for next-generation high-density optical disc storage. Kumagai says Sony's new blue-violet ultrafast pulsed semiconductor laser can emit 100 or 200 times more power than conventional laser diodes. In fact, this discovery can be a replacement for the titanium sapphire gas laser. Sony's plan is to use the ultrafast pulsed laser technology to generate high performance microscopes. Their goal is to combine old and new technologies to produce new products, such as advanced medical applications.

However, Sony is very reluctant to release more details about their new projects in these fields, particularly the technical details. In fact, Kumagai said he is the only one who is able to talk about these products which have been released and projects that have been made public since these details are wrapped in secrecy.

2.2 Signal Processing

2.2.1 Signal Detection

2.2.1.1 Forward Scattered Light

When laser light hits any particle, light is scattered in all angles. The light scattered in low-angle is called forward scatter which is the amount of light scattered in the forward direction as laser light strikes the cell. The magnitude of forward scatter is roughly proportional to the size of the cell, and this data can be used to quantify that parameter. Figure 25 shows how to convert scattered light to a quantified voltage.

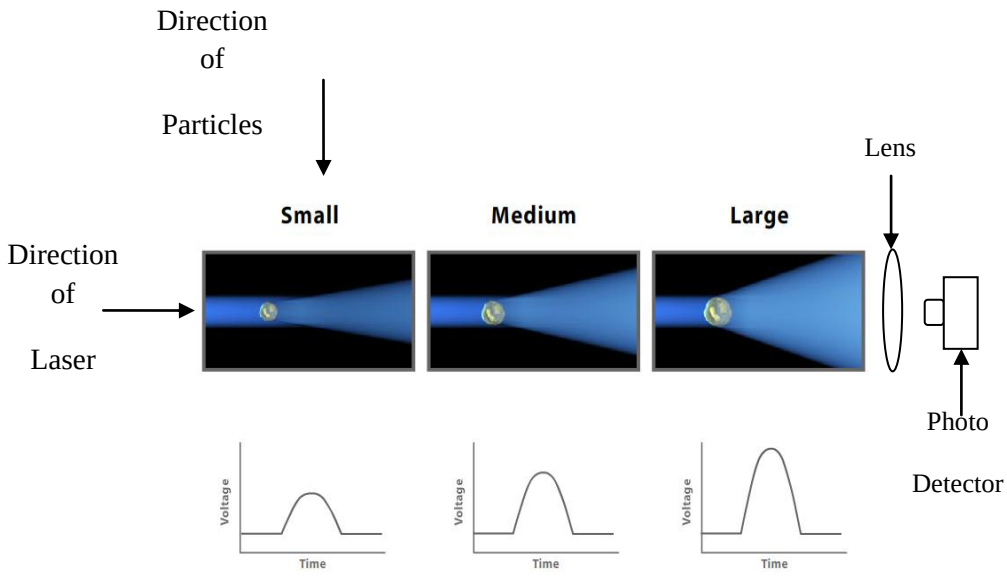

Figure 25: Size Comparison[20]

As it can be seen from Figure 25, the scattered light received by the detector (or PMT) is translated into a voltage pulse. In this figure, small cells produce a small amount of forward scatter and large cells produce a large amount of forward scatter. The scattered light is collected by a lens and focused into a photo detector and the magnitude of the voltage pulse recorded for each cell is proportional to the cell size.

One-Dimensional Histogram

A histogram of forward-scatter data is a graphical representation of the size distribution within the sample population[21], but this graph only represents one-dimensional data as shown in Figure 26.

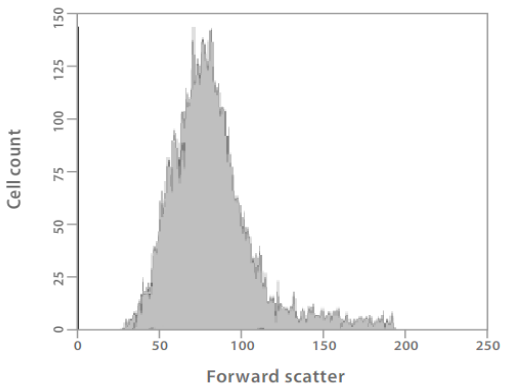

Figure 26: Forward Scatter Histogram[22]

Figure 26 represents a histogram of scattered data, at which smaller cells appear toward the left and larger cells appear toward the right. Therefore, in Figure 26, the majority of cells have sizes from 50 to 100 units and at the size of 70 units, almost 140 cells were detected.

Almost the same principle applied for forward scattering is applied for backward scattering, except that the light is reflected in backward direction (after the laser hits cells). After that, backward light is focused by a lens and goes to a photodiode (PMT) and then data is recorded in a similar way as in Figure 25 and Figure 26.

Forward scattered light follows Rayleigh and Mie scattering; when the diameter of a cell is much smaller than the laser wavelength, the cell practices a Rayleigh scattering[23]. However, when the diameter of a cell is larger than the laser wavelength, the cell practices Mie scattering[25]. Both types of scatterings will be discussed in the following part.

a. Rayleigh Scattering

Figure 27: Rayleigh Scattering[24]

Figure 27 shows the angular distribution of a Rayleigh scattering. When laser hits a particle with a diameter much smaller than the laser wavelength, a Rayleigh scattering occurs. The scattered laser intensity is distributed quite evenly in all direction around particles with a slight reduction in side scatter as illustrated in Figure 27. Since Rayleigh scattering intensity is inversely proportional to the wavelength, it affects low wavelengths more than the high wavelengths and this is why the sky is blue since the blue colour is at lower spectrum wavelength.

b. Mie Scattering

Mie scattering occurs when the diameter of a cell is larger than the laser wavelength. Mie scattering produces a pattern like an antenna lobe, with a sharper and more intense forward lobe for larger particles as shown in Figure 28.

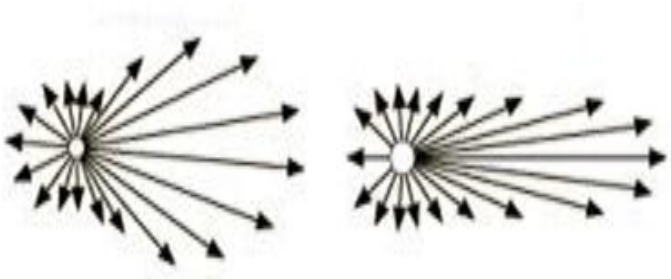

Figure 28: Mie Scattering for Small (left) and Large (right) Particles[24]

Mie scattering is not distributed in all angles equally as in Figure 27 for a Rayleigh scattering. Rather, the scattering looks like an antenna lobe, with a sharper and more intense forward lobe for larger particles as shown in Figure 28. Mie scattering is not like Rayleigh Scattering in terms of depending strongly on wavelength and this is why it produces almost white glare around the sun when a lot of particulate materials are present in the air[25].

2.2.1.2 Side Scattered Light

Any particle that passes through a laser beam scatters light at all angles. The light scattered in low-angle is called forward scatter which is the amount of light scattered in the forward direction as laser light strikes the cell. However, light scattering at larger angles is called side scattered light which is the amount of light scattered in the side direction as laser light strikes the cell. Side scattered light is

due to the granularity and structural complexity of the particle and it is focused by a lens and is collected by a side detector (or PMT) which is located 90 degrees from the laser's path. The signals collected by the side-scatter detector can be plotted on a one dimensional histogram like the forward scatter light discussed before.

Two-Dimensional Histogram

A one-dimensional histogram does not necessarily show the complexity of the cell or particle populations. To illustrate this idea, what seems be a single population in the forward scatter histogram, will be multiple populations in a second dimension. This is done by using a two-dimensional histogram as shown in Figure 29.

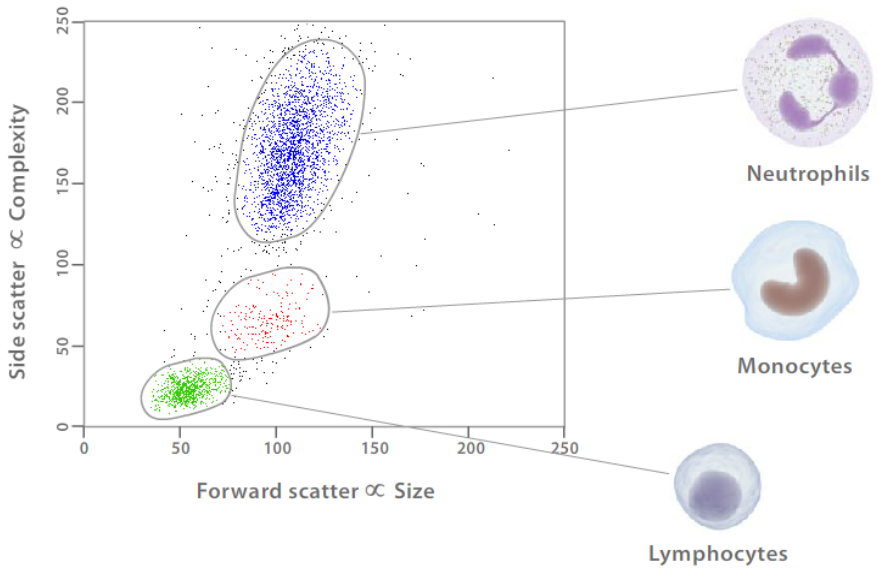

Figure 29: 2D Scatter Plot of Blood[26]

As it can be seen from Figure 29, the peaks from the forward and side-scatter histograms correlate with the coloured dots in the scatter plot. The populations that emerge include lymphocytes which are small cells possessing low internal complexity; monocytes which are medium-sized cells with slightly more internal complexity, and neutrophils and other granulocytes which are large cells that have a lot of internal complexity.

2.2.1.3 Fluorescence

Fluorescence is one of the most common ways to study cellular characteristics using flow cytometer including the use of fluorescent molecules such as fluorophore-labelled antibodies. Fluorescence is the excitation of a fluorophore to a higher energy level followed by the return of that fluorophore to its ground state with the emission of light. Figure 30 shows typical fluorescent energy levels.

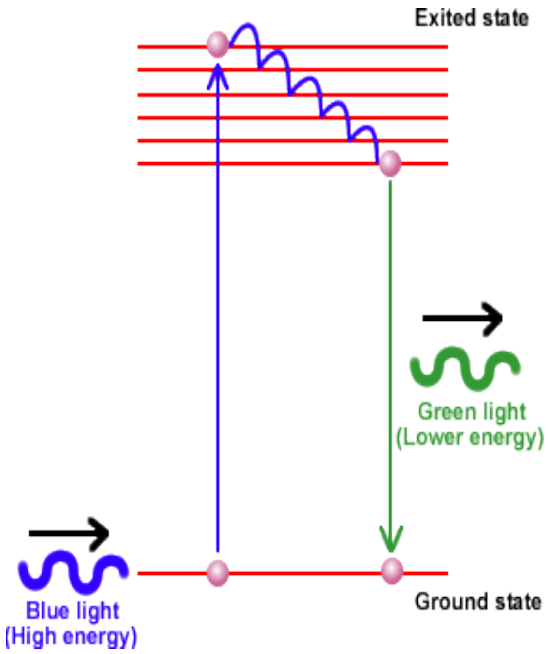

Figure 30: Energy State Diagram for Fluorescence[27]

As it can be seen from Figure 30, the fluorophore is excited to a higher energy level and then returns back to its ground state after emission of light. The energy in the emitted light depends on the energy level in which the fluorophore is excited and this light has a lower energy level and a larger wavelength (with a specific colour).

In the fluorescent detection method, often a labelled antibody is added to the cell sample. The antibody then binds to a specific molecule on the cell surface or inside the cell. After that, when laser light of the right wavelength hits the fluorophore, a fluorescent signal is emitted and detected by the side photo detectors (or PMT's) since the fluorescent light passes through the side scatter signal path[28].

Different Wavelength Detectors

As the fluorescent light passes through the side path, it is directed to a series of filters and mirrors, so that particular wavelength ranges are delivered to the appropriate detectors.

Fluorescence data is collected in the same way as forward and side scatter data as mentioned before. Some labelled cells will emit brighter light than others depending on their nature (dead, alive, male or female) since each cell passes the path of the laser, a fluorescence signal is generated. The fluorescent light is then directed to the appropriate detector where it is translated into a voltage pulse proportional to the amount of fluorescence emitted. These voltage signals are recorded and can be presented in graphs.

Two-Colour Experiment

In some cases, one laser source operating at a specific wavelength can excite two fluorophores. As a result, two colours can be detected from a single laser (this process is called a two-colour experiment). For example, the two fluorophores, Alexa Fluor® 488 and phycoerythrin (or R-PE) are commonly used together. They can be excited with a 488 nanometer laser light source and the emission peaks for these two dyes can be seen far enough from each other as shown in Figure 31 and Figure 32.

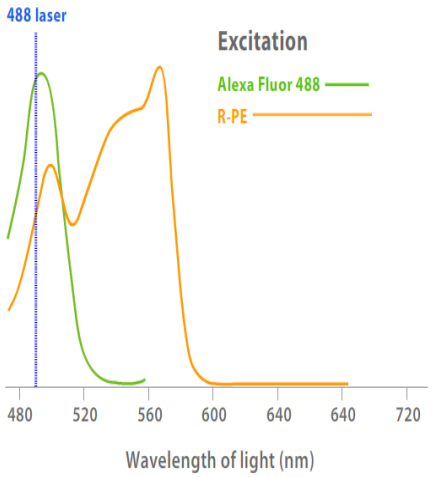

Figure 31: Two Colour Experiment (Excitation)[29]

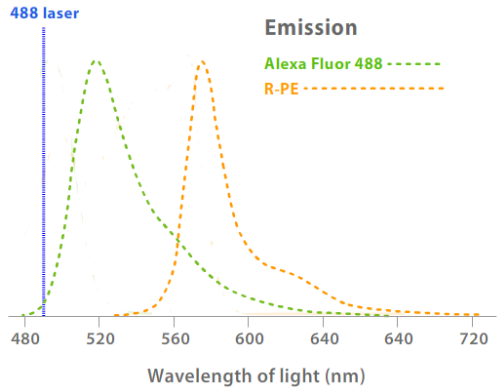

Figure 32: Two Colour Experiment (Emission)[29]

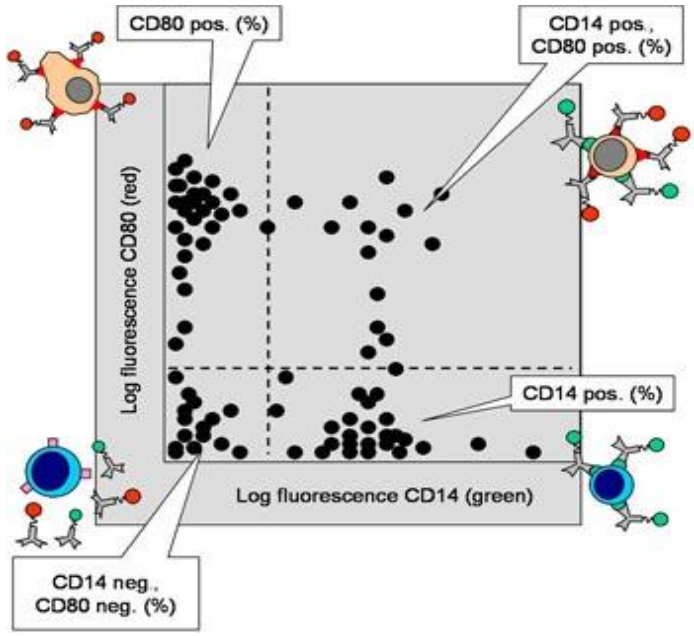

Figure 33: Two Colour Dot Plot[30]

Figure 33 shows a scatter plot for two colour experiment, four distinct populations emerge: cells with only bright orange fluorescence appear in the upper left quadrant, cells with only green fluorescence appear in the lower right quadrant, cells with both bright green and bright orange fluorescence appear in the upper right quadrant and finally, cells with both low green and low orange fluorescence appear in the lower left quadrant.

Using Filters

To collect discrete fluorescence data for the Alexa Fluor® 488 and R-PE fluorophores, optical filters are used. A 530nm bandpass filter is used to collect

the Alexa Fluor® 488 peak and a 585nm bandpass filter is used to collect the R-PE peak. So, proportional amounts of Alexa Fluor® 488 and R-PE fluorescence can be recorded for each cell. Sometimes portions of each emission peak overlap one another (this is called spectral overlap). Figure 34 shows different types of optical filters.

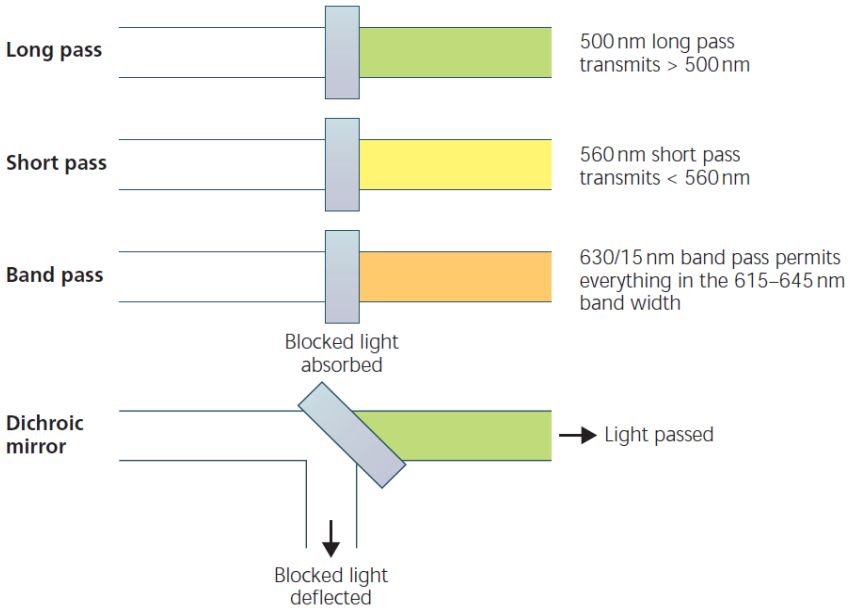

Figure 34: Different types of optical filters[31]

2.2.2 Signal Enhancement

In most cases, collected signals from scattering and fluorescence are weak even if they are detected by high sensitive PMT's and amplified. The collected signals must be enhanced in order to give accurate results. There are many methods used in signal processing to enhance collected signals and remove noise. Two of them will be discussed: phase contrast and Weiner filter methods. Phase contrast is used because of its advantage in determining the structural complexity of particles even for weak signals. Weiner filter method is used because it removes the noise created by the lenses and plates existing in the flow cytometers and pickups.

2.2.2.1 Phase Contrast Method

Phase contrast method is used to enhance signals and helps in giving more details about examined cells, such as their sizes and internal complexities. To illustrate this, when a beam is focused towards the cell, some of the beam hits the cell directly and some hits the edge of the cell and interferes with the other signal

which causes constructive or destructive interference (appears as black and white colours in the detector)[32]. Figure 35 and Figure 36 show both cases.

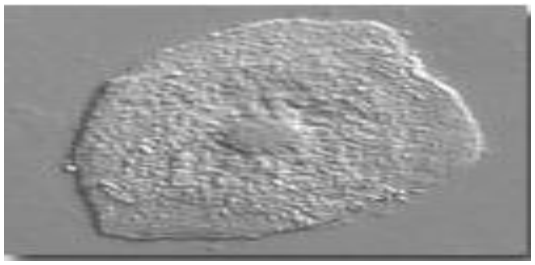

Figure 35: A picture taken without a contrast method[33]

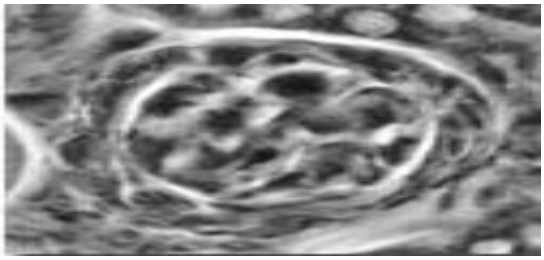

Figure 36: A picture taken with phase contrast method[33]

Figure 35 and Figure 36 were taken from the same cell. In Figure 35, there are not many details about the internal complexity of the cell but the image in Figure 36, which was taken using phase contrast method, shows many cell's details because the information taken from the beams hits the mid of the cell and the cell's edges, were used. This appeared as black and white colours due to constructive and destructive interference.

Phase contrast method uses unsharp mask filter (also called boost filtering). Mask filter subtracts a smoothed (or unsharp) version of an image from the original image to enhance the information on the edges according to equation (2)[21].

$$I_{edges}(x,y) = I_{original}(x,y) - I_{smoothed}(x,y) \quad (2)$$

Where I represents the image intensity and (x,y) represents a pixel coordinate.

After that, the resulting image from equation (2) is added to the original image to get an enhanced image with some degree of sharpening according to equation (3).

$$I_{enhanced}(x,y) = I_{original}(x,y) + kI_{edges}(x,y) \quad (3)$$

Where k is a constant scaling factor that ensures the resulting image is within certain limits and the edges are not 'oversharp'.

2.2.2.2 Weiner Filter Method

The Weiner filter method is another way to enhance weak collected signals. The commercial cytometers as well as the low cost cytometers have many lenses and optics that are used to gather and direct light. These lenses can be a source of noise because of their finite sizes; Weiner filter is used to eliminate this type of noise.

In theory, the field in the lens plane is the Fourier transform of the field in the photo diode plane. However, in real life this cannot be completely right because the lens size is finite and the image Fourier transform is truncated by the lens, or multiplied by a circular rect function[34]. Therefore, the effect in the photodiode plane is the convolution of the image of the object with the transform of the circular rect function, which is known as the "jinc" function. So, a blued signal is generated as in equation (4).

$$g(x,y) = f(x,y) \otimes h(x,y) \tag{4}$$

Where f is the original signal, h is point spread function (PSF) and g is the blurred signal (the scattered signal after passing through the lens).

If noise is added to equation (4), then equation (5) can be derived.

$$g(x,y) = f(x,y) \otimes h(x.y) + n(x,y) \tag{5}$$

Where n is noise.

If Fourier transform is taken to equation (5), then equation (6) is gained

$$G(u,v) = F(u,v)H(u,v) + N(u,v) \tag{6}$$

Where G (u,v) is the Fourier transform for the blurred signal with noise.

The estimated original signal can be calculated using equation (7).

$$\dot{F}(u,v) = \frac{G(u,v)}{H(u,v)} = \frac{F(u,v)H(u,v)+N(u,v)}{H(u,v)} = F(u,v) + \frac{N(u,v)}{H(u,v)} \tag{7}$$

Equation (7) shows the problem associated with the inverse filter. To elaborate this, when H(u,v) is close to zero, the estimate of F(u,v) will be swamped by a magnified version of the spectrum of the noise i.e. when F(u,v) is inverse transformed, these large values will be spread throughout the estimate of f(x,y). This shows the main drawback of inverse transform method and leads to the Wiener filter method which solves this issue.

The Wiener filter appears in equation (8).

$$W(u,v) = \frac{\dot{H}(u,v)}{|H(u,v)|^2 + \emptyset(u,v)} \tag{8}$$

Where $\emptyset$ (u,v) is an estimate of the spatial frequency dependent noise-to-signal ratio.

Since the spatial frequency dependence of the noise is often not known, it is often replaced by a constant.

If we put the equation of Wiener filter in equation (6), we get equation (9).

$$F(u,v) = G(u,v)W(u,v) = \dot{G}(u,v)\left(\frac{\dot{H}(u,v)}{|H(u,v)|^2+\emptyset}\right) = \frac{F(u,v)|H(u,v)|^2}{|H(u,v)|^2+\emptyset} + \frac{N(u,v)\dot{H}(u,v)}{|H(u,v)|^2+\emptyset} \tag{9}$$

From equation (9), when H(u,v) is large, we get equation (10).

$$\hat{F}(u,v) \approx F(u,v) + \frac{N(u,v)}{H(u,v)} \tag{10}$$

However, when H(u,v) is small, we get the following equation (11):

$$\hat{F}(u,v) \approx \frac{F(u,v)|H(u,v)|^2}{\emptyset} + \frac{N(u,v)\dot{H}(u,v)}{\emptyset} = \frac{\dot{H}(u,v)}{\emptyset}[F(u,v)H(u,v) + N(u,v)] = \frac{\dot{H}(u,v)}{\emptyset}G(u,v) \tag{11}$$

The noise in equation (11) is finite and small. So, the noise associated with the finite size of lens can be illuminated using Wiener filter.

2.2.3 The Use of a Threshold

There is some noise associated with flow cytometer's electronics, such as thermal and shot noises. Noise can also be generated by the information of the large number of minute particles (platelets and debris) which would dominate the data pool. To prevent this problem, a threshold level is set such that a certain forward

scatter voltage must be exceeded before the cytometer is able to collect data. Figure 37, shows a threshold level for blood cell run.

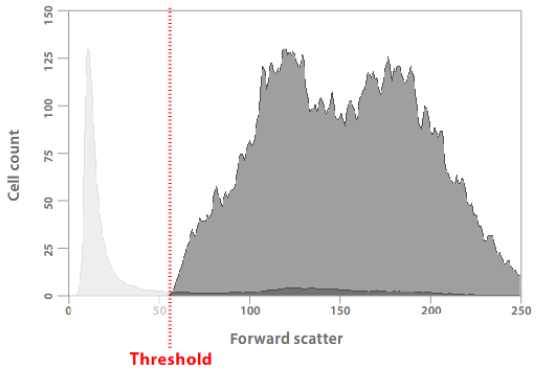

Figure 37: Threshold Level[20]

In Figure 37, a threshold level was created at 55 units in the forward scatter axis to not count small cells and noise. In this figure, the blank area represents noise, small cells and debris that are not considered because the pulse voltage they generate is less than the threshold level while the black area represents the actual data which is needed to be considered.

3. EXPERIMENTAL SETUP

3.1 Overview

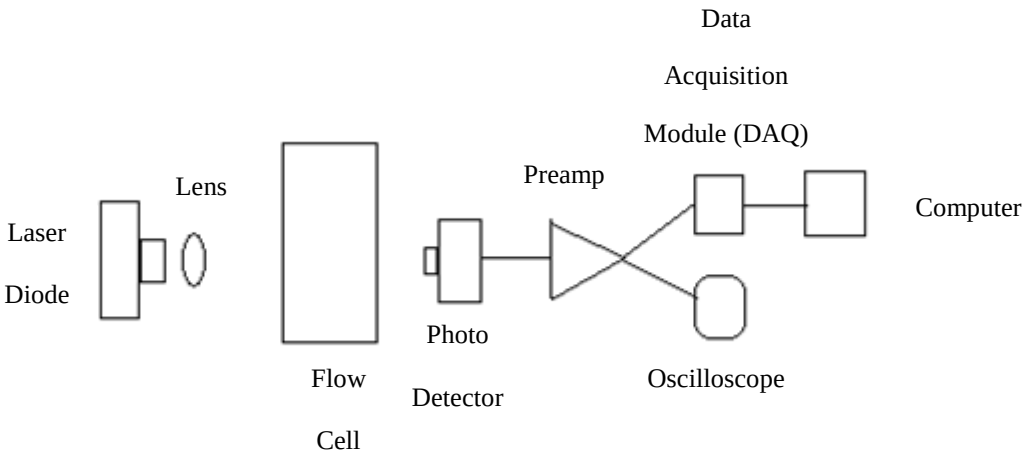

Figure 38: Blu-ray cytometer main setup diagram

Figure 38 shows the overview of the main Blu-ray cytometer: particles are poured in the syringe and move according to pump system selected settings. Then, a laser driver gives the required power to the laser diode in the Blu-ray pickup via a PCB interface board. Next, laser beam is focused to the flow chip's channel containing moving particles. On the other side of the flow chip's channel, a photo detector is located to receive the laser beam after hitting the stream of particles. This photo detector is connected to a pre-amplifier to amplify the received laser beam and it is connected to an oscilloscope and to a data acquisition module (DAQ) via coaxial cables. The oscilloscope shows the continuous laser signal as well as the scattered signal. The data acquisition module converts the electric signal from analog to digital and connects the digital signal to a computer in order to analyse the signals and count the particles.

Note: only forward and side scatter (fluorescence) signals were analysed and used in this thesis and no back scatter signals were used.

3.2 Illumination System

Figure 39: Laser diode driver

The illumination system consists of a laser diode driver, a PCB interface board and a laser diode. Figure 39 shows the laser driver used in this thesis. The laser driver type is LDC 500, ThorLabs. The DVD laser cathode was grounded and the current limit set to 36mA.

Operation of the Laser Driver

First, the power button and the enable button are switched ON. Then, the constant power mode is selected to have constant power even if there is a drop in the signal power. In the display window, the current limit is fixed to be 34mA in order to not burn the laser driver in the Blu-ray pickup.

Laser Diode

The laser diode used in these experiments is in the optical pickup (SF-BD413P) (Figure 24) and the Blu-ray pickup sled was removed from a Panasonic DMPBD45GN-K Blu-ray player. The blue ray wavelength is 405nm and the lens aperture is 0.8. Figure 40 shows the laser lens in the Blu-ray pickup; it also shows the flow chip. When the laser driver is ON, the laser beam in the Blu-ray pickup is focused by a lens into the flow cell.

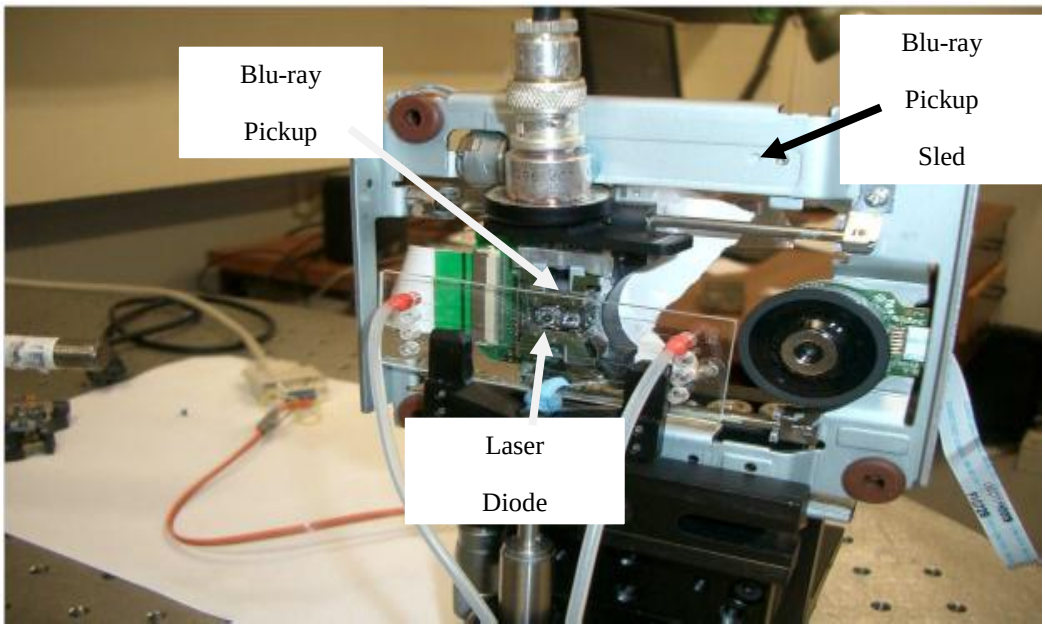

Figure 40: Laser Diode in the Blu-ray Pickup

PCB Interface Board

The PCB interface board connects the Blu-ray laser diode to the LDC 500 laser power supply. It was designed by Andrew Clow using Eagle™ software (CadSoft). The PCB was built by (www.pcbzone.co.nz), but was not populated with connectors[35]. An adapter board was made using the PCB from another pickup unit. Table 2 shows the mounting board pinout and Figure 41 shows the PCB inter face board circuit layout.

Table 2: Blu-ray Laser Mounting Board Pinout. Pin 1 is located closest to the ribbon cable connector on the optical pickup unit.

Blu-ray Mounting Board	Ribbon Cable	Laser Diode
1	Not connected. Goes to the photodiode for the red system	
2	GND e.g. Pin33	Pin C
3	Pin 32 LDI_BD	Pin B
4		
5	Pin 44 MD_BD	Pin A
not connected	Pin 45 GND_BDFPD	

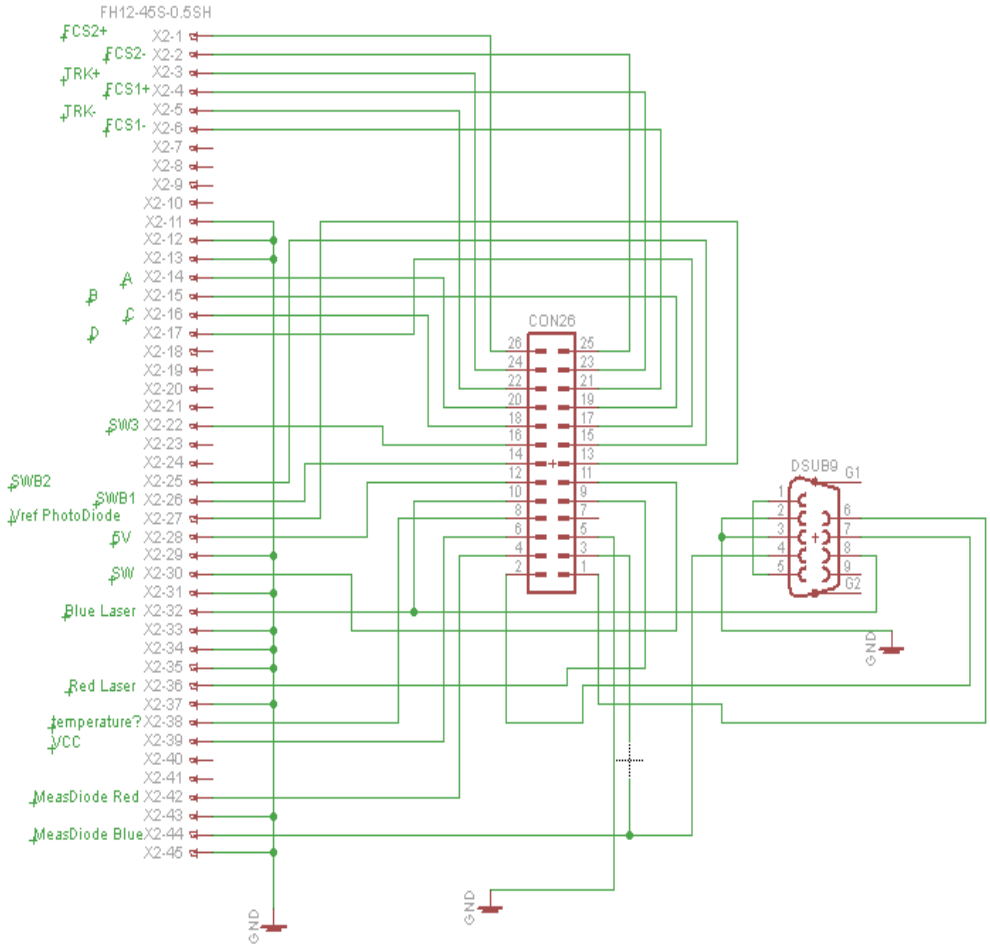

Figure 41: PCB Interface Board Circuit Layout[35]

3.3 Detection System

The detection system consists of a photo detector and a pre-amplifier. The photo detector part number is UDT PIN 10D (United Detector, Circular detector 11mm diameter). The Amplifier part number is DHPCA-100 (FEMTO, 105 V/A and 14MHz bandwidth). Figure 42 and Figure 43 show the photo detector and the pre-amplifier with their part numbers.

Figure 42: The Photo Detector

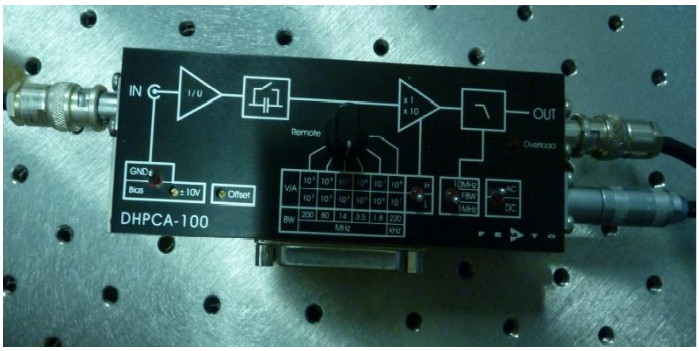

Figure 43: Pre-amplifier

Operation

After the laser beam is scattered from the particles, it is then collected by the photo detector. Because the photo detector is relatively large (11mm diameter), it collects most of the scattered laser which is then amplified by the pre-amplifier. The pre-amplifier is connected to an oscilloscope to show the laser scattered signals and is also connected to a data acquisition module (DAQ) which transmits the signals to a computer after converting them from analog to digital.

3.4 Fluidics System

Pump Systems

The fluidics system consists of pump systems and a flow cell. Two pump systems were used in these experiments, the old (Perfusor 6, manufactured by B. Braun) and the new (LabSmith's uProcess™) pump systems.

Old Pump System

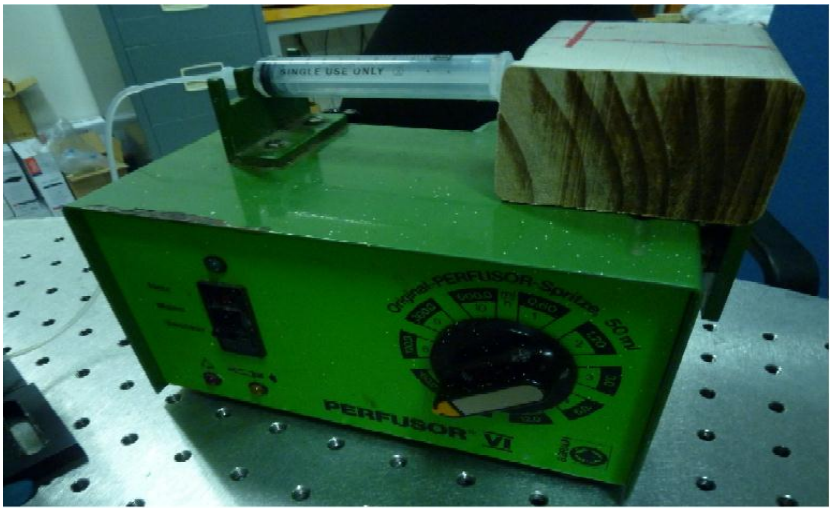

Figure 44: Old Pump System

Figure 44 shows the old pump system which consists of a syringe pump, 10ml syringe and an adapter. It has 10 settings and each one has a different speed. Table 3 shows the settings versus their flow rates.

Table 3: Pump Rates for 10ml Syringe

Setting Number	10ml Syringe (µl/s)
1	0.045
2	0.09
3	0.22
4	0.45
5	0.9
6	2.25
7	4.5
8	9
9	22.5
10	45

The New Pump System

The new pump system is LabSmith's uProcess™ which is a platform comprised of a suite of hardware and software products that simplify construction and control of microfluidic systems. The new pump system has many advantages over the old one, such as great control of the flow rate that can be controlled through programming and any speed can be selected. Figure 45 shows an image of the overall system, Figure 46 shows how to open or close valves and Figure 47 shows how to increase or decrease the flow rate of the particles.

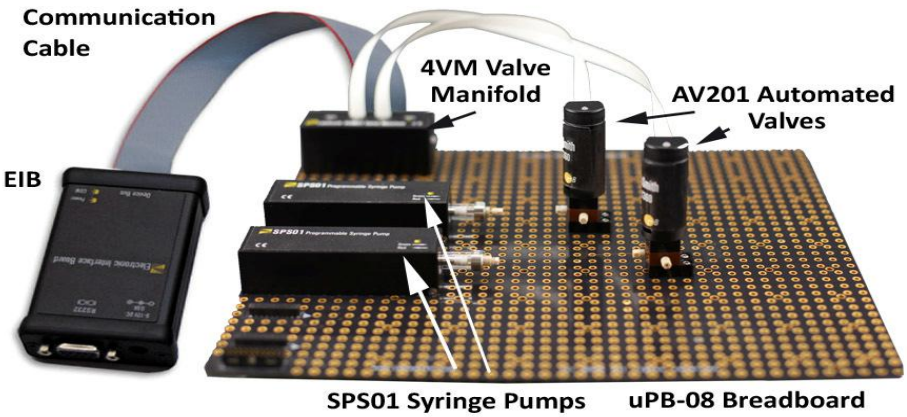

Figure 45: New Pump System Components.

The new pump system consists of the following main parts:

1. Breadboards: for positioning and mounting automated uDevices and CapTite components.
2. Syringe Pumps: for programmable metering of micro- volumes.
3. Automated Selector Valves: They have two positions and three port automated selector valves.
4. Valve Manifold: for interfacing up to four automated selector valves
5. Electronic Interface Board: for interfacing automated uDevices and uProcess software.
6. One-Piece Ferrules and Plugs: to connect capillary or tubing to components.
7. Tubing Size Adapters: to use capillary or tubing with components of a different size.
8. Reservoirs: On-chip or on-breadboard fluid storage.
9. Luer-Lock™ Adapter: to connect pumps and syringes: to capillary or tubing.
10. Capillary and Tubing: for capillary and tubing in 360um, 1/32" and 1/16" ODs.

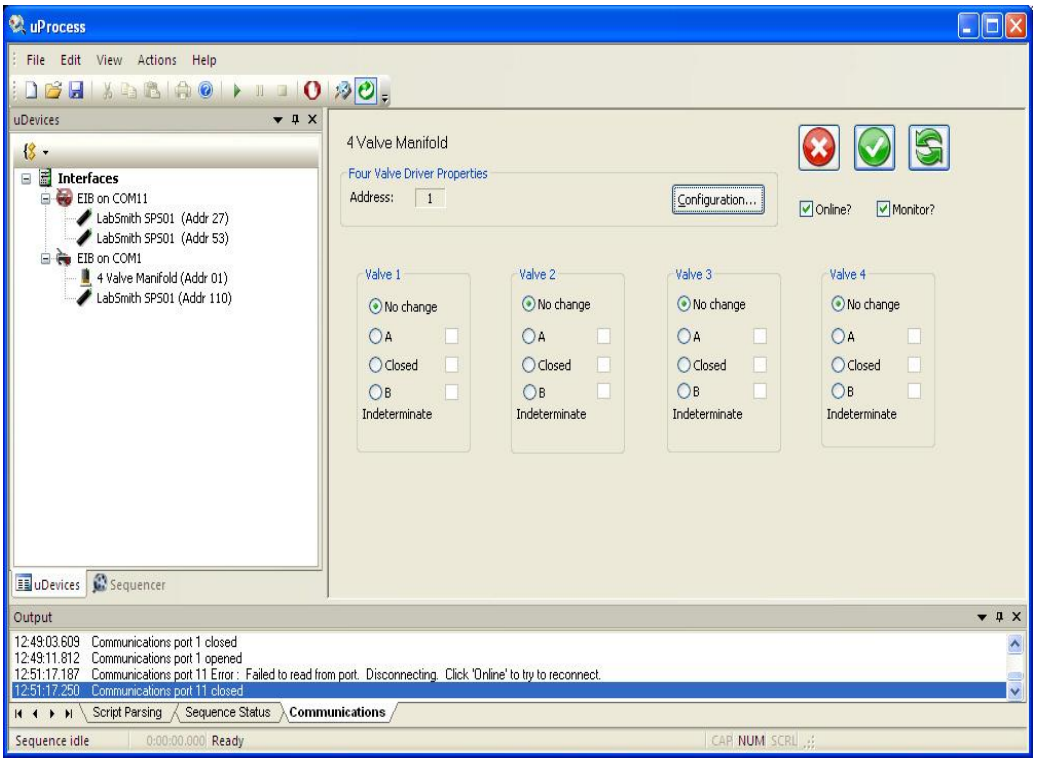

Figure 46: Control Panel for Valve Manifold.

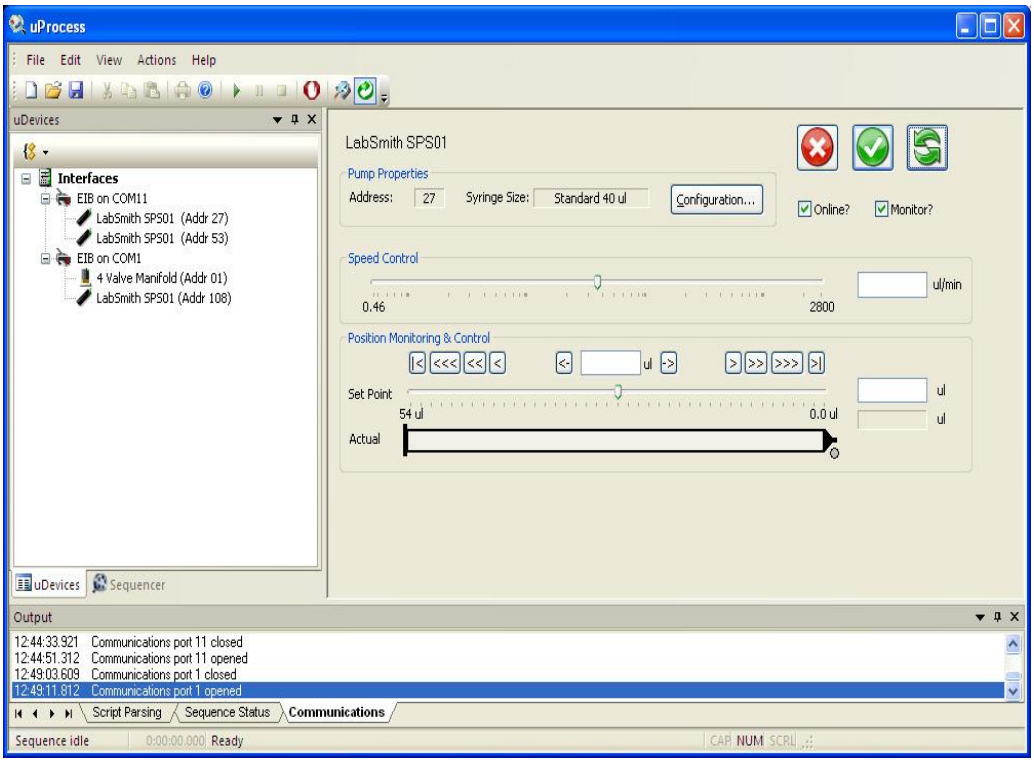

Figure 47: Control Panel for Syringe Pump.

Flow Cell

The flow cell is a plastic channel through which particles can pass through for some measurements to be taken. It looks like a thin line or a strand of hair. To view the flow cell really closely, a microscope has to be used. The micro flow cell used in this project is a Topas chip. This chip contains 4 parallel 100µm by 100µm channels (Microfluidic ChipShop). One disadvantage of this chip is that the material it is made from is quite soft so it can get scratched easily. Figure 48 shows the flow cell used in these experiments and the upper channel (number 1) was used for the particles to pass through.

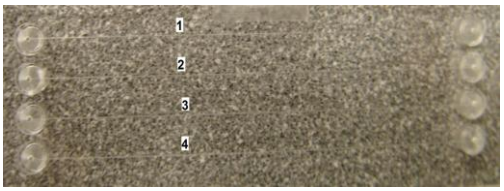

Figure 48: Topas Chip 4 Parallel Flow Cells

3.5 Data Analysis and Computer System

3.5.1 Data Acquisition Module (DAQ)

The data acquisition module (DAQ) used in this project is National Instruments USB-6259 BNC. It is an analog to digital converter and capable of 1MS/s sampling at 16 bit resolution. It is a high performance M Series multifunction DAQ optimised for superior accuracy at fast sampling rates. It has 16 analog inputs, 4 analog outputs, 8 digital input/output, 2 APFI and 2 user defined BNC terminals and it is connected to a PC via a USB port.

The National instrument USB 6259 BNC was used in combination with LabView™ automation and control software and a Microsoft Excel™ spreadsheet to analyse and count trapped particles. The raw voltages from the detectors were imported into an Excel™ spreadsheet from the analogue to digital converter. A sample rate of 10 kHz was used and the number of samples and different parameters can be programmed using the LabView program. A coax cable is connected from the amplifier to pin “Al 0, FS” in the output board and a USB cable is connected from the DAQ to a PC.

A threshold level was selected for detecting particles greater than the noise floor. A lockout time (1ms) was implemented to prevent false triggering due to the diffraction grating causing multiple pulses for a single particle.

Three trials were conducted with the diffraction lines parallel with the fluid flow and the trials were repeated with the diffraction lines perpendicular to the fluid flow. The threshold voltage for the last four tests was 0.01V. Varying the threshold voltage did not change the count very much. Figure 49 shows the data acquisition system and the connected coax cable to pin "Al 0, FS" in the output board.

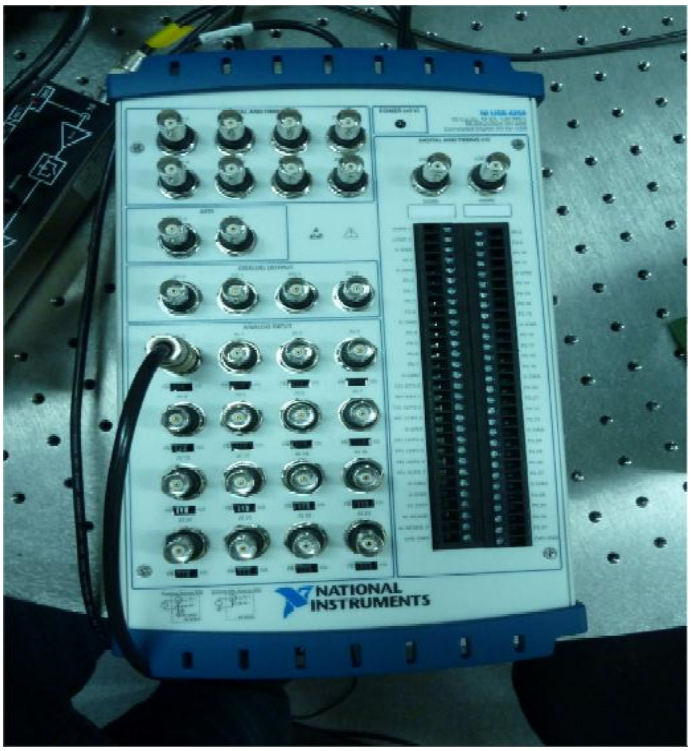

Figure 49: The data acquisition module (DAQ)

3.5.2 LabView Design and Analysis

3.5.2.1 Calculating the Set Point for Threshold Level

As mentioned in section (2.2.3), there is some noise associated with flow cytometer's electronics, such as thermal and shot noises. To eliminate this noise, a threshold level is set such that a certain forward or side scatter voltages must be exceeded before the cytometer is able to collect data. A threshold level was selected for detecting particles greater than the noise floor.

According to Watson, the light intensity profile across a laser beam is Gaussian (or normal) distribution[20]. After many trials in this thesis, it was found that 3 standard deviations added to the mean give the best threshold level and therefore the most accurate particles' count. So, equation (12) was created to calculate the set point for the threshold level.

$$The\ set\ point = \mu + 3\sigma \tag{12}$$

Where μ is the mean value and σ is the standard deviation.

One standard deviation (σ) covers 68.2% of the information in the examined signal, 2σ covers an additional 27.2% and 3σ covers an additional 4.2% of the data in the desired signal. So by choosing 3 standard deviations (3σ), 99.6% of the data is covered[36].

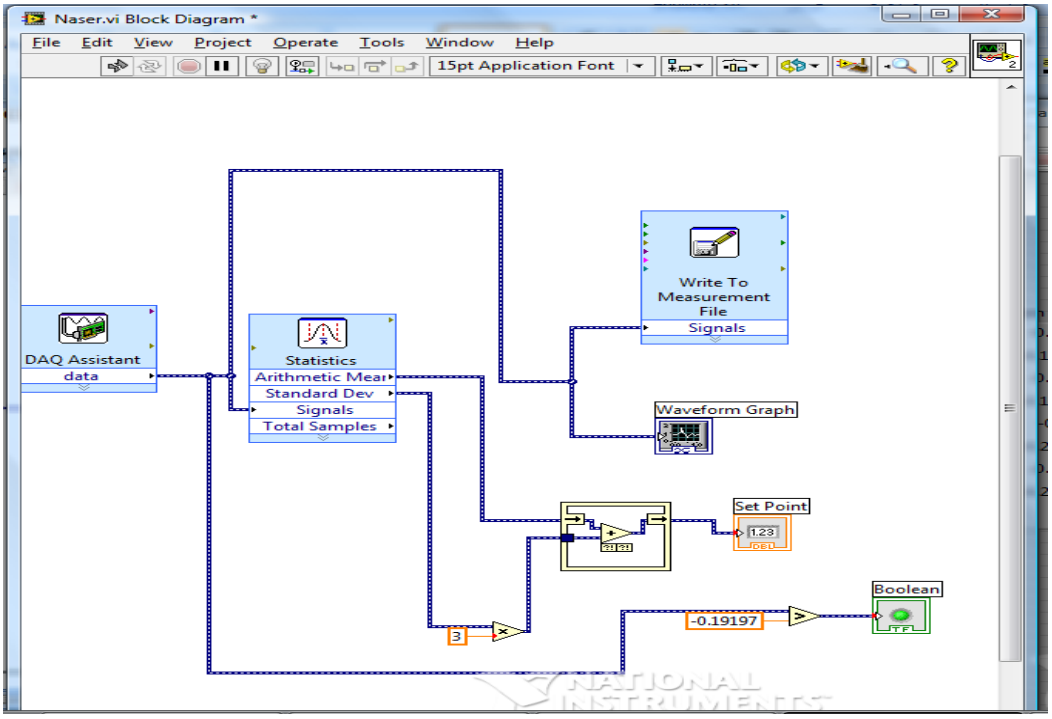

Figure 50: LabView program calculating the set point

Figure 50 shows the LabView block diagram and it was created to measure the set point for the threshold level. A DAQ assistant block was installed to acquire data from the DAQ module. After that, the output from DAQ assistant block is connected to a statistics block which can calculate the mean and the standard deviation. Then, the standard deviation is multiplied by 3, added to the mean and the result is compared to each sample data. It gives '1' if the data is greater than

the result and gives ’0’ otherwise. The data is written to an Excel spreadsheet using a ’Write To Measurement File’ block and the data is plotted using ’Waveform Graph’ block. The Boolean button can give a green light each time a particle is detected.

3.5.2.2 Automatic Counting

To count particles, a LabView program was created as in Figure 51 and Figure 52. First, a ’DAQ Assistant’ block was created to acquire data from the DAQ Module. The comparator block compares the sample signal to the set point and gives ’1’ if the data signal is greater than the set point and gives ’0’ otherwise. A detection of ’1’ means that a particle is detected. After that, ’Case Structure' was created to count the detected particles. The output of the comparator is inputted into the ’case structure’ as a control. When the control is ’1’, the case structure performs the true case ’Figure 51’ and adds ’1’ to the shift register. On the other hand, when the control is ’0’, the ’case structure’ performs the false case ’Figure 52’ and keeps the previous value of the shift register.

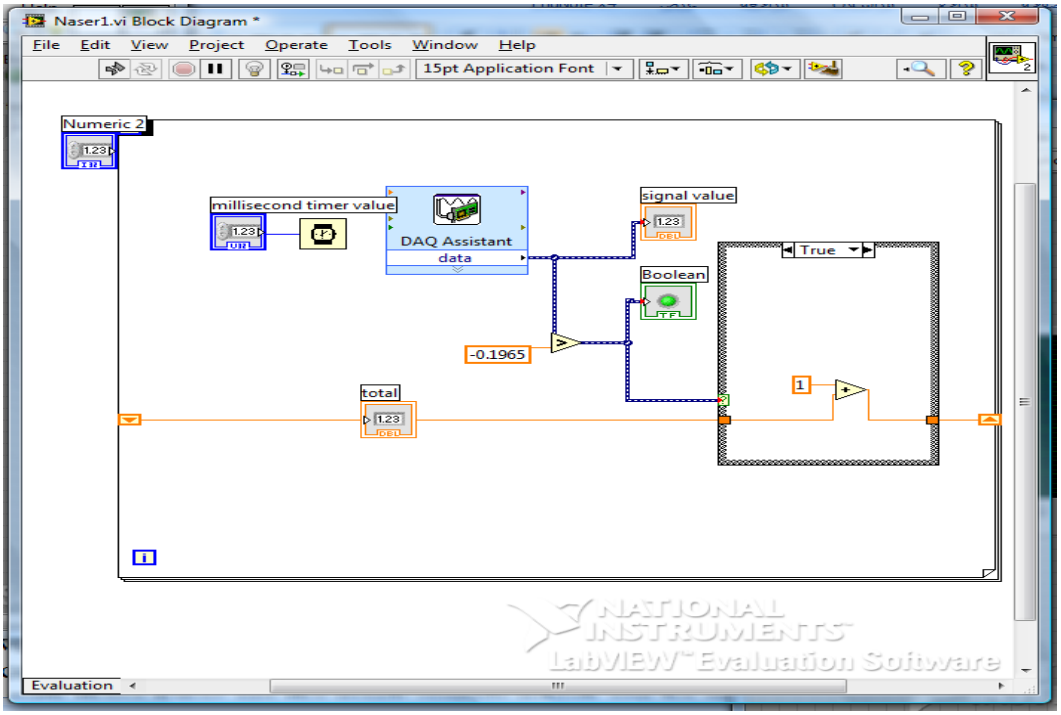

Figure 51: LabView Program for Automatic Counting (true case)

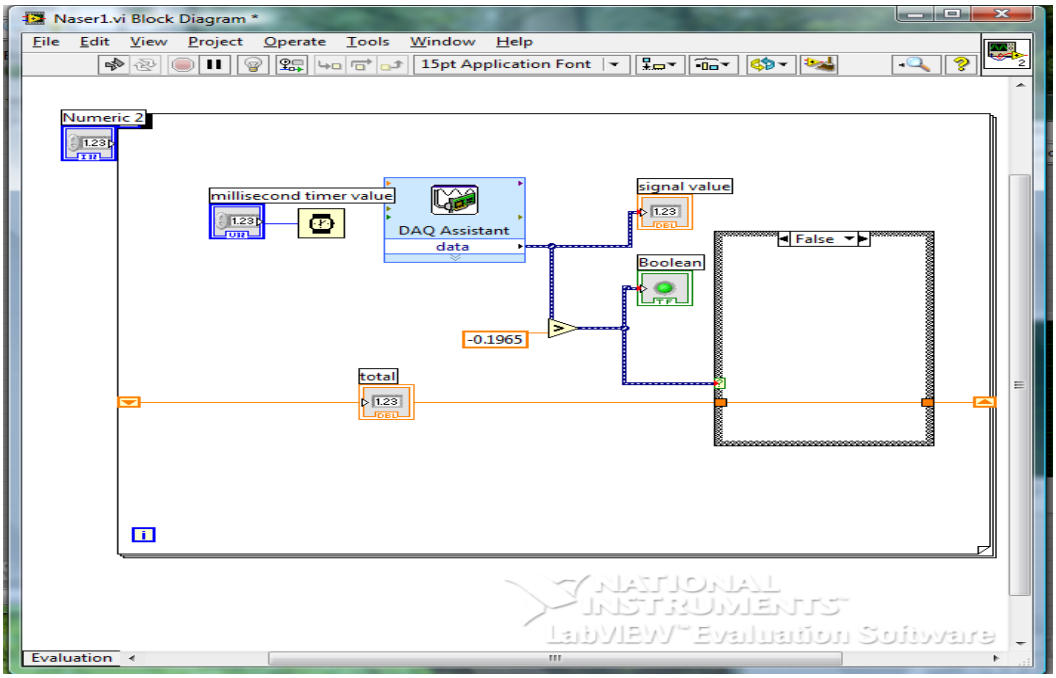

Figure 52: LabView Program for Automatic Counting (false case)

3.5.2.3 Creating Two Channels in LabView

Two channels were created in LabView to count the detected particles from the forward and side detectors at the same time. Figure 53 shows the block diagram of the LabView program and Figure 54 shows the data obtained from the LabView in an Excel spreadsheet.

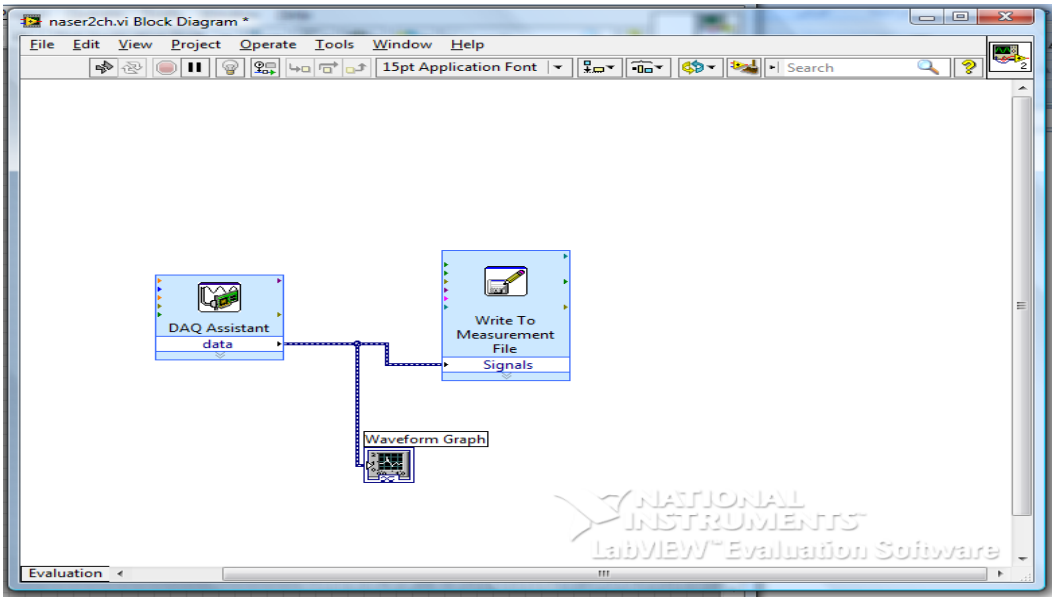

Figure 53: LabView Program for creating two channels in Lab view

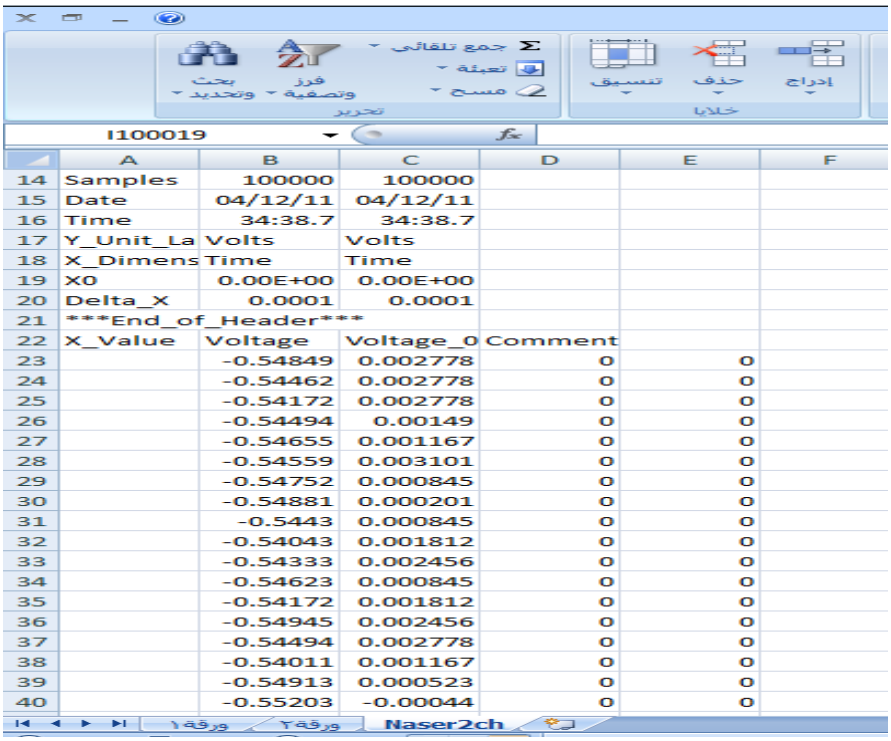

I100019

	A	B	C	D	E	F
14	Samples	100000	100000			
15	Date	04/12/11	04/12/11			
16	Time	34:38.7	34:38.7			
17	Y_Unit_La	Volts	Volts			
18	X_Dimens	Time	Time			
19	X0	0.00E+00	0.00E+00			
20	Delta_X	0.0001	0.0001			
21	***End_of_Header***					
22	X_Value	Voltage	Voltage_0	Comment		
23		-0.54849	0.002778	0	0	
24		-0.54462	0.002778	0	0	
25		-0.54172	0.002778	0	0	
26		-0.54494	0.00149	0	0	
27		-0.54655	0.001167	0	0	
28		-0.54559	0.003101	0	0	
29		-0.54752	0.000845	0	0	
30		-0.54881	0.000201	0	0	
31		-0.5443	0.000845	0	0	
32		-0.54043	0.001812	0	0	
33		-0.54333	0.002456	0	0	
34		-0.54623	0.000845	0	0	
35		-0.54172	0.001812	0	0	
36		-0.54945	0.002456	0	0	
37		-0.54494	0.002778	0	0	
38		-0.54011	0.001167	0	0	
39		-0.54913	0.000523	0	0	
40		-0.55203	-0.00044	0	0	

Naser2ch

Figure 54: the data obtained from LabView in Excel Sheet

As it can be seen in Figure 54, two voltage columns were created in an Excel spreadsheet, one is for the forward detector and the other is for the side detector. The other two columns ’0’s’ in Figure 54 represent the detected particles.

3.5.3 MATLAB Program

After building all the required programs in LabView, it was noticed that for low flow rates, detected particles were counted more than once. This is because the detected signal is wide for slow speed. When sampling a wide signal, many ’1’s can be counted for one particle. To solve this issue, a MATLAB program was created to delete the duplicated ’1’s. It was very difficult to do this in LabView because all programs were built in LabView and it was difficult to change all blocks in the LabView programs and add this programming part. Moreover, MATLAB is very good at data comparison and the writer of this thesis has a better understanding in MATLAB programming. The following program is the MATLAB program used for this issue:

```
x = load ('APD20s9.txt');        % load data into vector y

% removing multiple signal detections

for i=1:99995
```

```
        if x(i)==x(i+1)
            x(i+1)=0;
        end
        if x(i)==x(i+2)
            x(i+2)=0;
        end
        if x(i)==x(i+3)
        x(i+3)=0;
        end
        if x(i)==x(i+4)
        x(i+4)=0;
        end
        if x(i)==x(i+5)
        x(i+5)=0;
        end
end
```

As seen from the MATLAB program, the signal data is loaded to a vector ’y’ and each data is compared with the next five data. If ’1’ is detected, the next ’five samples’ are converted to ’0’ in order to not be counted again. Five samples were chosen based on the data for low flow rates.

4. EXPERIMENTAL PROCEDURES AND RESULTS

In this chapter, some conducted experiments are discussed; they were done using the existing system. Some modifications and developments to the existing system have been made, too. In addition, a new setup using an avalanche photodiode (APD) will be discussed in detail.

4.1 Counting Accuracy of 20µm Particles with and without a Beam Stop

4.1.1 Design

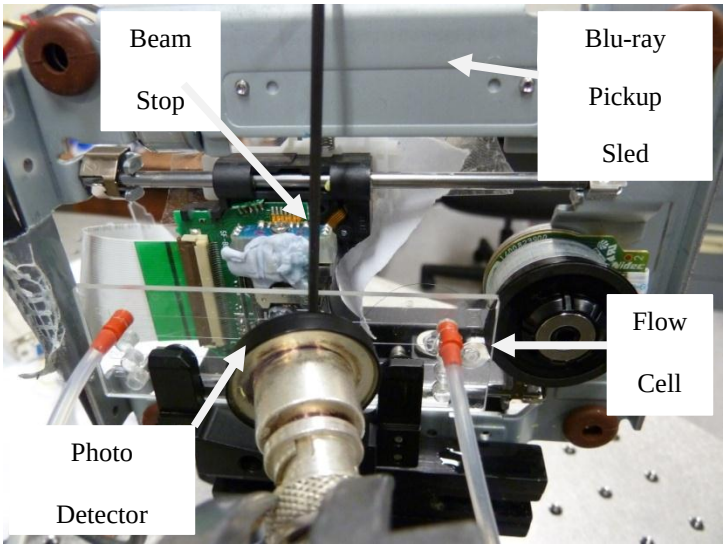

Figure 55: A Picture of the Main Circuit for Counting 20µm Particles Using a Beam Stop

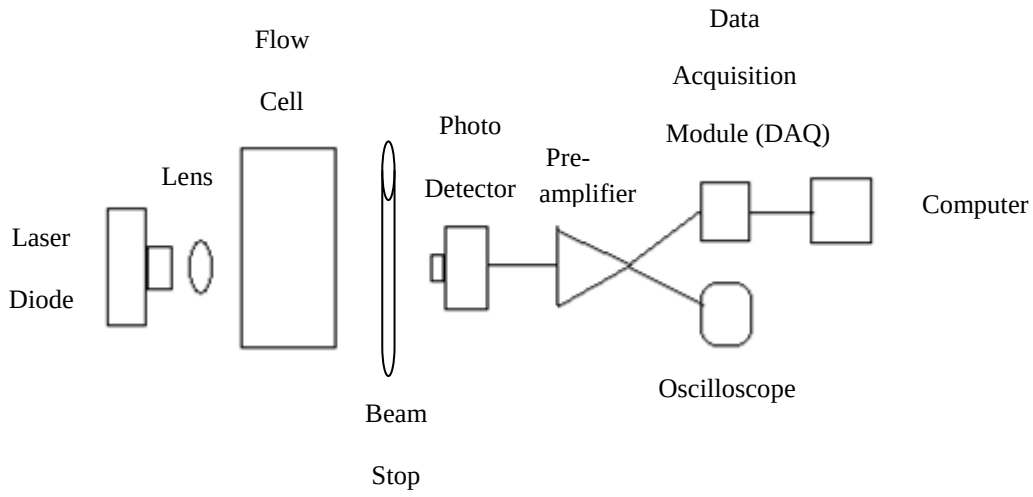

Figure 56: A diagram of the Main Circuit for Counting 20µm Particles Using a Beam Stop

In this part, a beam stop was installed in front of the photo detector as shown in Figure 55 and Figure 56.There are two main purposes to installing the beam stop; the first one is to record a reduction in the signal when a particle passes instead of

recording an increase in the signal like what has been done by other researchers. The second purpose is to check if Mie theory (see section 2.2.1.1) can be applied for our particles using this system.). The particles used in this part are 20µm diameter, 3000 particles per ml, latex spherical beads and their category number is CC20 (Count- Cal™, Thermo Scientific). Figure 57 shows the beam stop used in this part (cylindrical shape, 1.5mm diameter).

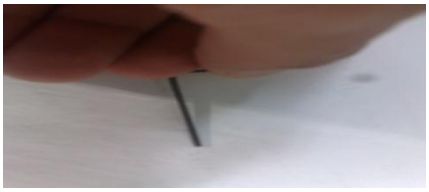

Figure 57: A Beam Stop

4.1.2 Results and Discussion

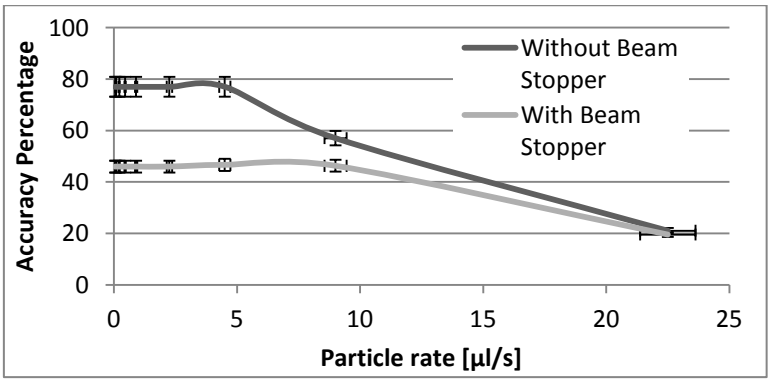

Figure 58: Percentage of Counting Accuracy of 20µm Particles with and without a Beam Stop

Figure 58 shows that the percentage of counting accuracy was better without a beam stop (~80%) and drops at 5µl/s. However, it was only ~40% by using a beam stop. This may be because particles mostly scatter laser signals in the forward direction and produce a pattern like an antenna lobe according to Mie theory (see section 2.2.1.1). When a beam stop is installed in front of the photo detector, the beam stop prevents most of the scattered laser signals from propagating in the forward direction and being detected by the photo diode.

The counting accuracy is the ratio (in percent) of the measured count to the actual one. The actual count is measured by sucking particles from vials by a 2.5µl pipet and then dilute them in distilled water. For example, Figure 58 shows that at a rate

of 9µl/s, the theoretical number of the particle is 270 and the measured number of particles is 154, so the percentage will be (154/270)*100=57%.

The vertical error bars in Figure 58 represent the minimum and maximum values of 5 repeated measurements. The horizontal error bars show the pump flow error of 7% [35]. Two additional independent errors need to be considered: the calibration error (10%), that is the accuracy of the reference standards, and the pipetting error (5%). The total independent error then is $\sqrt{0.1^2 + 0.05^2} = 11\%$.

4.2 Counting Accuracy of 20µm Particles with a Beam Pass

4.2.1 Design

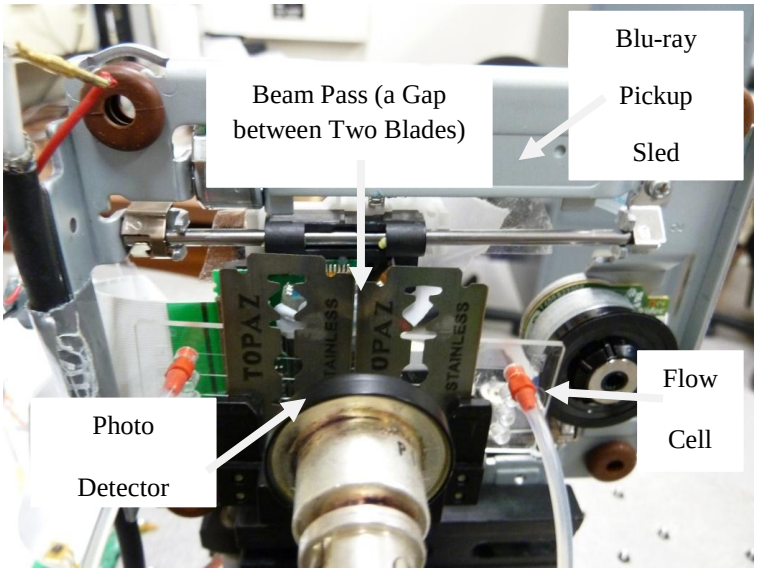

Figure 59: A Picture of the Main Circuit for Counting 20µm Particles Using a Beam Pass

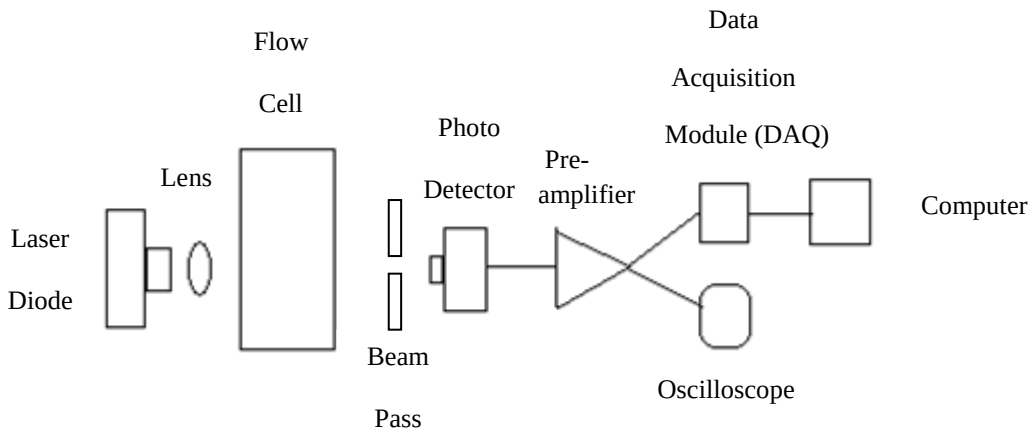

Figure 60: A diagram of the Main Circuit for Counting 20µm Particles Using a Beam Pass

In the last section (section 4.1), it was shown that the percentage of counting accuracy with a beam stop (~40%) was lower than the one without a beam stop (~80%). It was also mentioned that this may be because particles mostly scatter laser signals in the forward direction and produce a pattern like an antenna lobe according to Mie theory. In this part, however, a beam pass is intalled in front of the photo detector with the expectation that most scattered signals from particles will be detected by the detector because most of them should be in the forward direction. The beam stop was formed by a 1.5mm gap between two blades. Figure 59 and Figure 60 show the main circuit for counting particles using a beam pass. The particles used in this part are 20µm diameter, 3000 particles per ml, latex spherical beads and their category number is CC20 (Count- Cal^{TM}, Thermo Scientific).

4.2.2 Results and Discussion

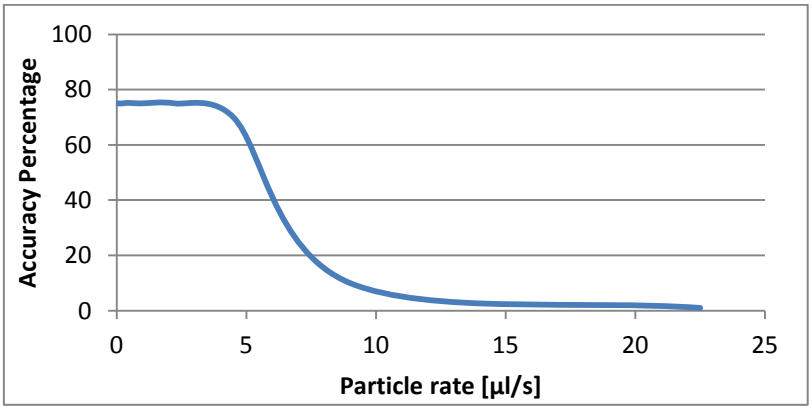

Figure 61: Percentage of Counting Accuracy of 20µm Particles with a Beam Pass

Figure 61 shows that the percentage of counting accuracy using a beam pass; it is ~75% and drops at 5µl/s. However, this percentage is much better than the percentage of counting accuracy using a beam stop (~40%) and it is almost the same as the percentage of counting accuracy without uing a beam stop (~80%). The 5% difference in percentage accuracy when using a beam pass (~75%) and without using it (~80%), may be because some scatter signals were blocked by the blades.

4.3 Counting Accuracy of 20µ Particles using normal Photodiode and APD

4.3.1 Design

In this experiment, the aim was to compare the quality of counting particles when using an avalanche photodiode (APD) and when using a normal photodiode to detect forward scattered laser signals. This is because the APD has a better sensitivity and a higher gain (40-100) than a normal photo diode. The particles used in this part are 20µm diameter, 3000 particles per mL, latex spherical beads and their category number is CC20 (Count- Cal™, Thermo Scientific). Figure 62 and Figure 63 show the experiment setup.

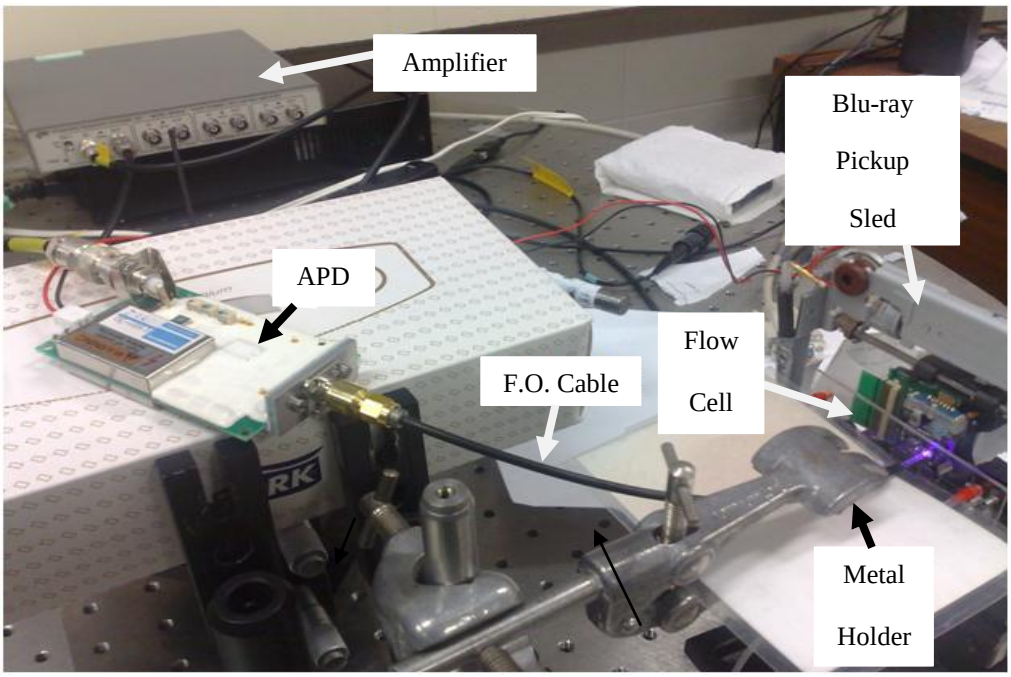

Figure 62: A Picture of the Main Setup for Forward Scattering using APD

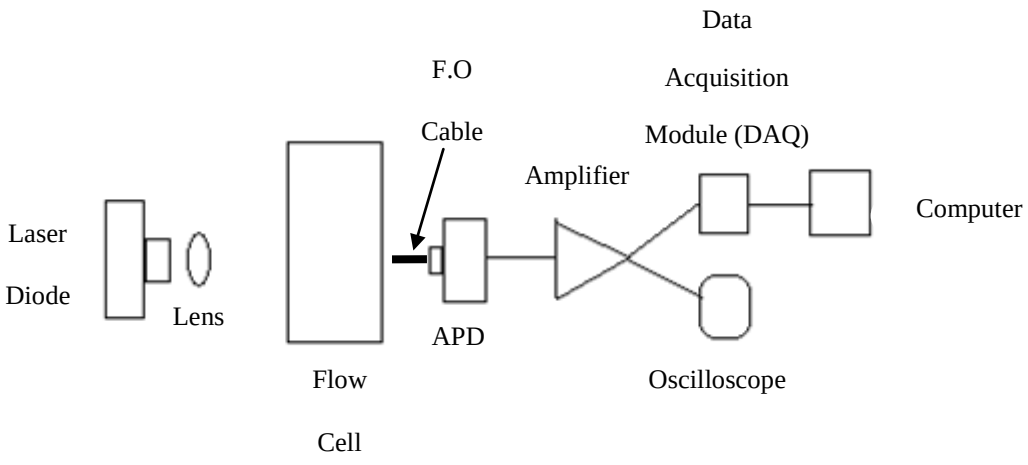

Figure 63: A diagram of the Main Setup for Forward Scattering using Normal Photodiode and APD

4.3.2 Results and Discussion

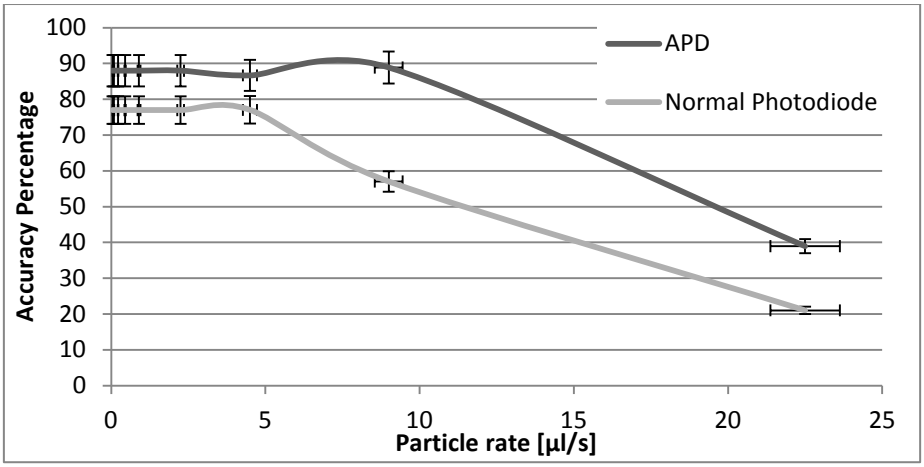

Figure 64: Percentage of Counting Accuracy of 20µm Particles using normal Photodiode and APD

Figure 64 shows that the accuracy percentage of counting particles is ~80% (drops at 5µl/s) when using a normal photo diode (same result as section 4.1.2). However, this percentage has been improved (~90%) when an avalanche photodiode was used.

This is because the APD has a higher sensitivity and gain than the normal photo diode. There might be some signal loss in the termination between the F.O. cable and the APD that counters this higher gain. An additional light loss might be due to some scattered light to not reaching the F.O. cable. This problem is minor because the diameter of the F.O. cable is quite large (1.5 mm) and it was very close to the flow cell (they almost touch each other). In section 4.1.2, 1.5mm beam stop made the percentage of counting accuracy very small (40%). So, the 1.5 mm F. O. cable seems to be able to detect most of the scattered signals since particles mostly scatter laser signals in the forward direction and produce a pattern like an antenna lobe according to Mie theory (see section 2.2.1.1). This is why the percentage of counting accuracy using an APD is higher than the one with a normal photo diode though the diameter of the normal photo diode is much larger than the diameter of the F.O. cable. Better results may be gained if the F.O. cable was attached to the flow cell instead of being close to it. In that case, a matching index material must be used between the F.O. cable and the flow cell to reduce any losses in the signal due to the difference in refractive index between air and glass.

4.4 Counting Accuracy Dependence on Focus

4.4.1 Design

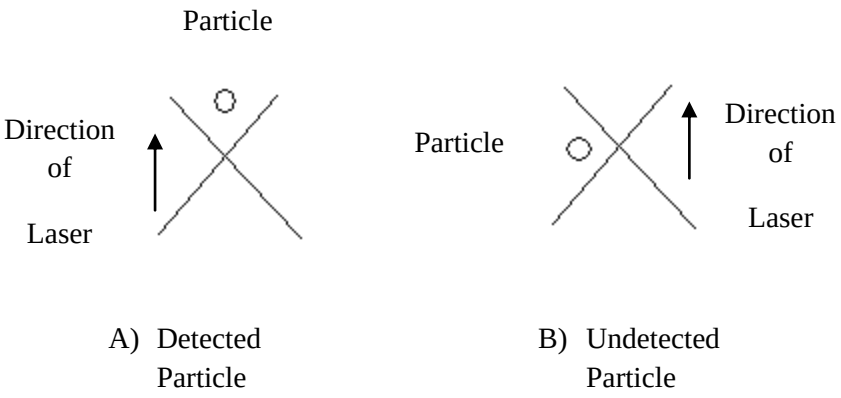

Figure 65: Particle detection for difference laser focus, particles flow perpendicular to the paper

The purpose of this experiment was to show the relationship between different lens focuses and the counting accuracy. As it can be seen from Figure 65 particle A was detected because it passed through the path of the laser beam whereas particle B was not detected because it did not pass through the path of the laser beam. This is due to the fact that the size of the particles is 20µm whereas the blue laser spot is as small as 0.5µm and the size of the channel is 100µm, which means that the particles can be anywhere in this wide channel. (N.B. the exact size of the laser spot can be measured using the knife edge test)[14].

In order to perform the experiment, the focus of the laser beam was set to two different positions and the percentage of accuracy for different flow rates was calculated. In the beginning, the laser spot was focused to the channel and was adjusted until the two channel's walls had been seen. After that, the distance was adjusted until the two walls of the targeted channel were aligned to the edge of the laser spot to maximise the area of laser beam hitting the whole area of the channel. After data was recorded, a slight change to the focus (0.05mm closer to the pickup) was made and another data was taken. The laser diode driver was set to 30mA and to a constant power. The particles used in this part are 20µm diameter, 3000 particles per ml, latex spherical beads and their category number is CC20 (Count- Cal^{TM}, Thermo Scientific).

4.4.2 Results and Discussion

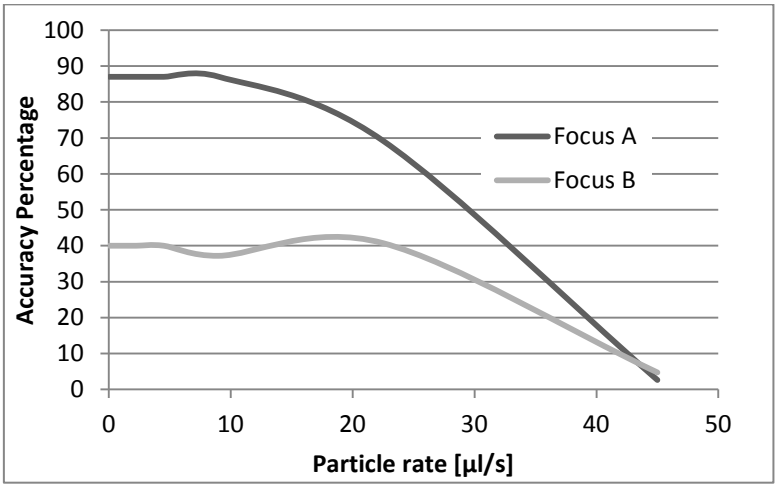

Figure 66: Percentage of Counting Accuracy of 20µm Particles for Two Different Focuses

Figure 66 shows the percentage of counting accuracy of 20µm particles for different flow rates. It shows that for two different foucuses A and B, there is a big change in the counting accuracy though the difference in distance adjustment between the two focuses was very slight (0.05mm). However, both curves show that the percentage accuracy decreases with the increace of the flow rate and this is because the particles go very fast, so, the photo detector could not catch all scatterd light from particles for high speed.

In section 4.1, the the percentage of accounting accuracy for 20µm particles was ~80% and it dropped at 5µl/s. On the other hand, in this section, the percentage is much better (~90%) and it dropped at a faster speed (10µl/s). This may be because the electronics used in this setup are too sensitive to light and the PC screen and the torch were switch ON when section 4.1 experiments were conducted but they were switched OFF when this section's experiments were conducted.

Something must be mentioned here: according to the human eye the position of focus B was much better than the position of focus A but according to the data it was the other way around which means that many focuses must be adjusted in order to take an optimal accounting accuracy; personal vision and adjustment should not be fully trusted.

4.5 Counting Accuracy of a Mixed of Fluorescent and Non-Fluorescent Particles

4.5.1 Design

In this part, fluorescent particles were counted for different flow rates and for forward scattering as well as for side scattering (for fluorescence detection). After that, the counting accuracy per different flow rates was done for non-fluorescent particles alone. After that, both types of particles were mixed together in one syringe (in order to go through one channel) and two photo detectors were connected to the system. The first detector detects the forward scattering for the fluorescent and non-fluorescent particles, and the second detector detects the side scattering for the fluorescent particles. Moreover, two channels were also created in the LabView program.

The purpose of this experiment was to see if the counting accuracy of one type of particles changes or remains the same when the particles are counted alone and when they are mixed with another type of particle. The second aim of this part is to see if a number of particles counted in the forward and the side scatterings are the same for the fluorescent particles.

4.5.2 Results and Discussion

4.5.2.1 Non-Fluorescent Particles Counting

In this part, the non-fluorescent particles will be counted when they are alone and not mixed with the florescent particles. The particles which were used in this experiment were 10μm particles. This diameter of particles was selected because the fluorescent particles diameter is 9.9μm. Therefore, both types of mixed particles have almost the same size and the same probability of detection. The laser diode driver was set to 30mA and to a constant power. The particles used in this part are 10μm diameter, 0.1% w/v, latex spherical beads and their category number is SL10L (Latex Calibration Particles, ProSciTech).

Calculation of the Number of Particles per Volume

To calculate the number of particles per unit volume, the following procedures must be followed:

For a weight/volume percentage of 1%:

$$1\% = \frac{1g}{100ml}$$

The density of latex is about 920 to 960 kg/m^3or 0.96 g/cm^3

$$\rho = \frac{0.94g}{cm^3} = \frac{0.94x10^{-3}kg}{10^{-6}m^3}$$

The mass of spheres per volume of liquid as specified on particles' vial= 0.1% = $\frac{0.1g}{100ml}$

$$\rho_{w-v} = \frac{0.1g}{100ml} = 1\frac{kg}{m^3} = \frac{1x10^{-4}kg}{100ml}$$

Mass of one sphere:

r=5µm, $v = \frac{4}{3}\pi r^3 = 5.236x10^{-13}L = 5.236x10^{-16}m^3$

$$M = \rho.v = 4.922x10^{-13}kg$$

Total mass of latex per volume of liquid chosen, 1µL:

$$M_{latex} = \rho_{w-v}.10^{-3}mL = 1x10^{-9}kg$$

$$N_{sphere} = \frac{M_{latex}}{M} = 2.032x10^3$$

The Results

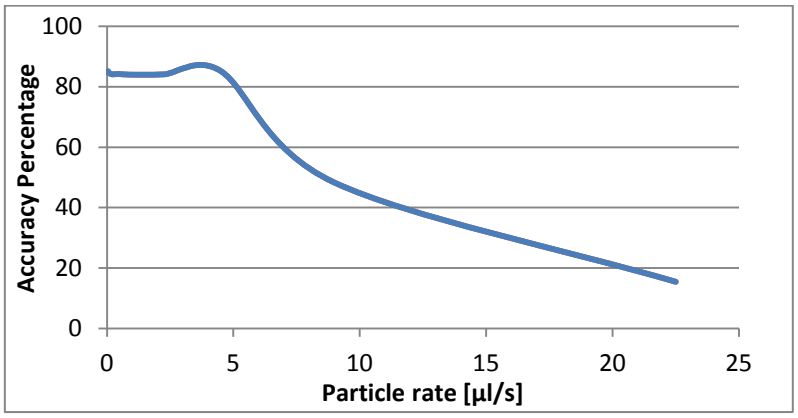

Figure 67: Percentage of Counting Accuracy of 10µm Particles

Figure 67 shows the percentage accuracy of 10µm non-fluorescent particles; as it can be seen from this figure the percentage of counting particles is ~85% and it drops at 5µl/s. However, the percentage of counting particles was ~90% and it drops at 10µl/s in section 4.4.2 but that was for 20µm particles. So, when the particles' size decreased from 20µm to 10µm, the percentage accuracy and the rate at which it drops also dereased.

Table 4: Experimental Calculations for Counting Accuracy of 10µm Particles

Setting	Exp.	Rate(µl/s)	Actual	%Count
1	8	0.045	9	85
2	15	0.09	18	85
3	38	0.22	45	84
4	77	0.45	91	84
5	154	0.9	183	84
6	385	2.25	457	84
7	779	4.5	914	85
8	883	9	1829	48
9	706	22.5	4572	15

Table 4: shows the experimental calculations for counting accuracy of 10µm particles. This table shows that the maximum number of particles at a rate of 22.5µl/s is less than 5000 particles/s. The data acquisition system used in this project has a maximum sampling rate of 100,000 samples/second. If the sampling rate is close to the maximum number of particles, then there might be some uncounted particles. However, in this case this issue didn't exist.

4.5.2.2 Fluorescent Particles Counting

The particles which were used in this experiment were fluorescent microspheres, 9.9µm in diameter. Their best excitation wavelength is 468nm and their emission green wavelength is 508nm. The dyes are incorporated into the polymer matrix (not surface dyed). The laser diode driver was set to 30mA and to a constant power. The fluorescent particles used in this part are 9.9µm diameter, 1% solids, latex spherical beads and their category number is G1000B (Fluoro- Max^{TM}, Thermo Scientific).

Calculation of the Number of Particles per Volume

Volume of one sphere:

r=4.95µm, $v = \frac{4}{3}\pi r^3 = 5.08x10^{-16}m^3 = 5.08x10^{-10}cm^3 = 5.08x10^{-13}L$

Mass of one sphere:

As specified on particles' vial, they have a density (ρ) of 1.06 g/cm^3

1.06 g → $1cm^3$

M → $5.08x10^{-10}cm^3$

$M = \rho.v$=$(5.08x10^{-10})$(1.06) = $5.3810^{-10}g = 5.3810^{-7}mg$

As specified on particles' vial, the spheres are packed as aqueous suspensions at 1% solids by weight. This means that 100mg liquid contains 99mg water and 1mg spheres (factor of10^{-2}).

Total mass of latex per volume of liquid chosen, 1µL (=1mg):

$N_{sphere} = \frac{10^{-2}}{5.38x10^{-7}} = 185873.$

The Results

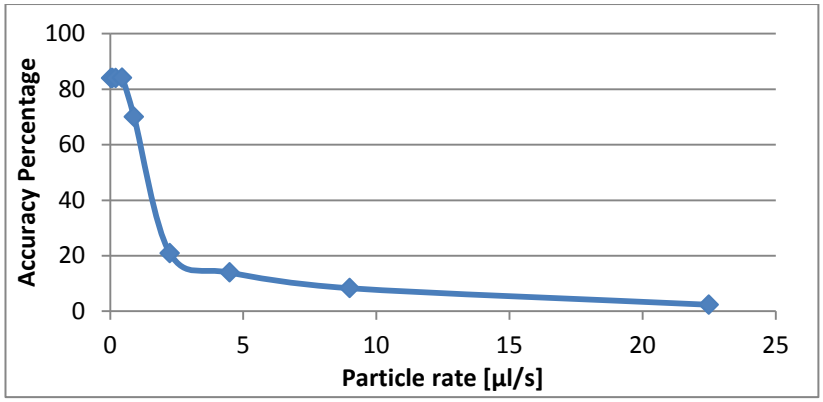

Figure 68: Percentage of Counting Accuracy of Fluorescent Particles

Figure 68 shows the percentage of counting accuracy for the 9.9µm fluorescent particles. As it can be seen from this figure the percentage of counting particles is ~85% and it drops at 1µl/s. However, the percentage of counting particles was ~80% and it drops at 5µl/s for the 10µm non-fluorescent particles. They have the same counting accuracy but it dropped faster when using fluorescent particles. This may be because the maximum number of particles is much higher in this case (less than 50,000 particles/s) than in the non-fluorescent case (less than 5,000 particles/s). It was very difficult to mix equal quantities from the two types of particles because the concentration of the non-fluorescent particles in the particles' vial is only 2,032 particles/µl whereas it is 185,873 particles/µl in the fluorescent particles' vial.

Table 5: Experimental Calculations for Counting Accuracy of Fluorescent 9.9µm Particles

Setting	Exp	Rate(µl/s)	Rate(mg/s)	Actual	%Count
1	70	0.045	0.045	83	84
2	140	0.09	0.09	167	84
3	343	0.22	0.22	407	84
4	701	0.45	0.45	833	84
5	1166	0.9	0.9	1667	70
6	867	2.25	2.25	4167	21
7	1159	4.5	4.5	8333	14
8	1380	9	9	16667	8
9	971	22.5	22.5	41667	2

Table 5 shows that the maximum number of particles at a rate of 22.5µl/s is less than 50,000 particles/s. The data aquisition system used in this project has a maximum sampling rate of 100,000 samples/second. If the sampling rate is close to the maximum number of particles, there might be some uncounted particles. However, the counting accuracy (~85%) drops faster for the fluorescent particles (at 1µm/s) than for the non flourescent particles (at 5µ/s). This may be because of the high number of flourescentt particles (<50,000 particles /s) which is very high compared to the number of non-fluorescent particles (<5,000 particles /s).

4.5.2.3 Fluorescent and Non-Fluorescent Particles Counting

In this part, fluorescent particles were counted for different flow rates and for forward scattering and side scattering (for fluorescence detection). After that, the counting accuracy per different flow rates was done for non-fluorescent particles alone. After that both types of particles were mixed together in one syringe (in order to go through one channel) and two photo detectors were connected to the system. The first detector is for the forward scattering and it detects the fluorescent and non-fluorescent particles and the other detector is for side scattering and it detects the fluorescence of the fluorescent particles. Moreover, two channels were also created in the LabView program.

The purpose of this experiment was to see if the counting accuracy stays the same or changes when one type of particle is counted alone or mixed with another type of particle. Moreover, it was meant to see if the forward and side scattering are the same for the fluorescent particles.

The Results

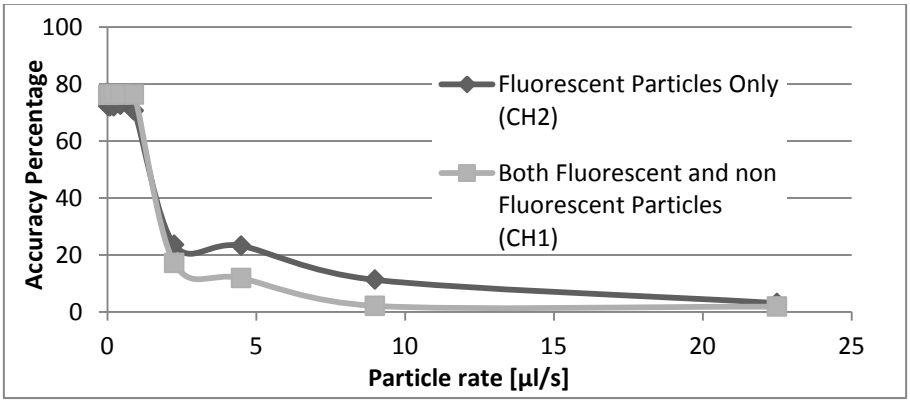

Figure 69: Percentage of Counting Accuracy of a Mix of 10µm Fluorescing and Non-Fluorescing Particles

As seen in Figure 69 mixing fluorescent and non-fluorescent particles decreases the percentage accuracy from ~85% (for both types of particles when they counted alone) to ~75% when they are mixed together. This percentage drops at 1µl/s though it was 5µl/s for the non-fluorescent particles when they were counted alone. This might be because the emissions of the fluorescent particles may hit other non-fluorescent particle, scatter and not reach the detector.

Table 6: Experimental Calculations for Counting Accuracy of a Mix of 10µm Fluorescing and Non-Fluorescing Particles

Set	Exp. ch1	Exp. ch2	Rate (µl/s)	Rate (mg/s)	Actual ch1	Actual ch2	% Count ch1	% Count ch2
1	67	63	0.045	0.045	92	83	72	76
2	133	127	0.09	0.09	185	167	72	76
3	326	310	0.22	0.22	452	407	72	76
4	671	635	0.45	0.45	925	833	73	76
5	1305	1271	0.9	0.9	1850	1667	71	76
6	1089	716	2.25	2.25	4624	4167	24	17
7	2148	992	4.5	4.5	9248	8333	23	12
8	2086	361	9	9	18495	16667	11	2
9	1459	792	22.5	22.5	46239	41667	3	2

As seen in Table 6, the maximum number of non-fluorescent particles at a rate of 22.5µl/s is less than 5,000 particles/s and the maximum number of fluorescent particles at a rate of 22.5µl/s is less than 50,000 particles/s, the ratio is 1:10. The data acquisition system used in this project has a maximum sampling rate of 100,000 samples/s. If the sampling rate is close to the maximum number of particles, there might be some uncounted particles. However, the high number of particles rate (50,000 particles /s) compared with the DAQ sampling rate might be the reason for the reduction in the counting accuracy from ~85% to ~75%.

4.6 Counting Accuracy for Fluorescence Particles as Forward Scattering and Fluorescence Detection with and without Filtering

4.6.1 Design

In this experiment, the percentage of counting accuracy for the fluorescence particles was measured when a 520nm green band-pass interference filter (Part # 520DF20) was placed over the photo-detector to prevent scattered light reaching it. In addition, the counting accuracy for the fluorescent particles was measured without filtering in order to compare it with the measurement taken using a filter. Finally, the fluorescent particles were counted as forward scattering not as fluorescent scattering. Figure 70 and Figure 71 show the experimental setup. It should be noted that the fluorescence life time is about 10ns. . The fluorescent particles used in this part are 9.9µm diameter, 1% solids, latex spherical beads and their category number is G1000B (Fluoro- MaxTM, Thermo Scientific).

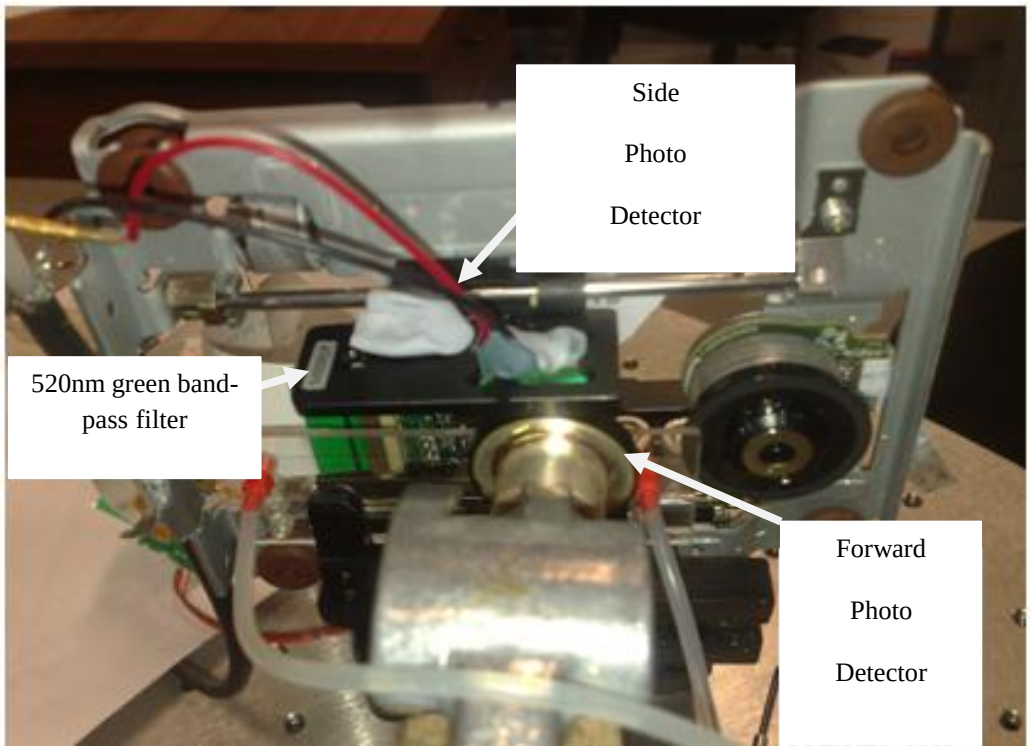

Figure 70: A picture of the Main Circuit for Forward Scattering and Fluorescence Detection with and without Filtering

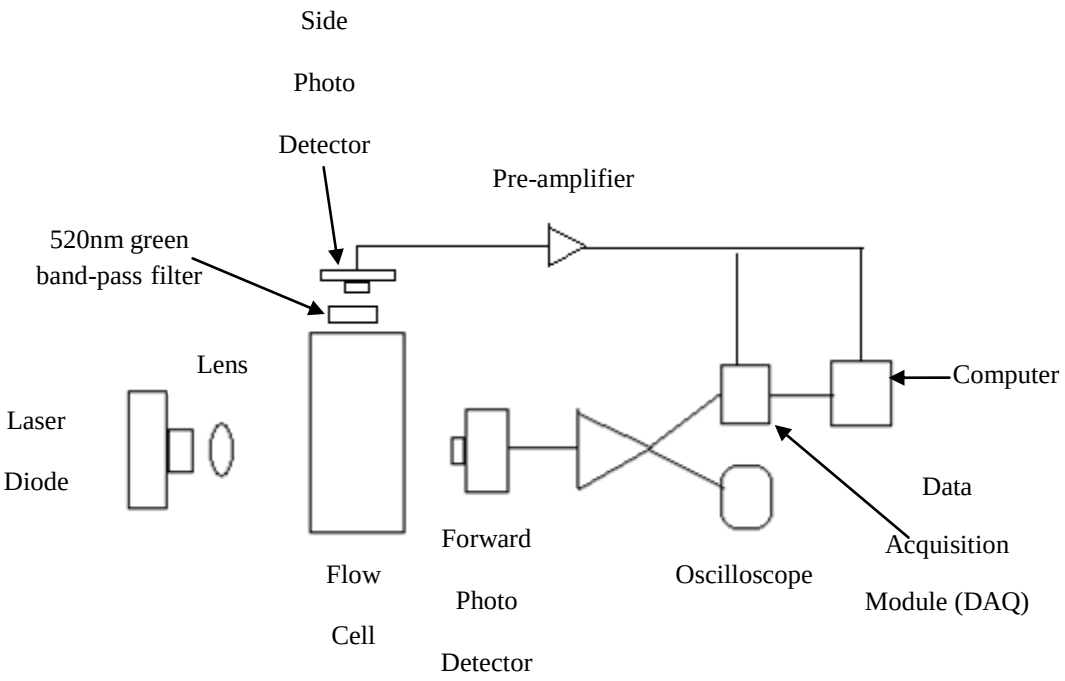

Figure 71: A diagram of the Main Circuit for Forward Scattering and Fluorescence Detection with and without Filtering

4.6.2 Results and Discussion

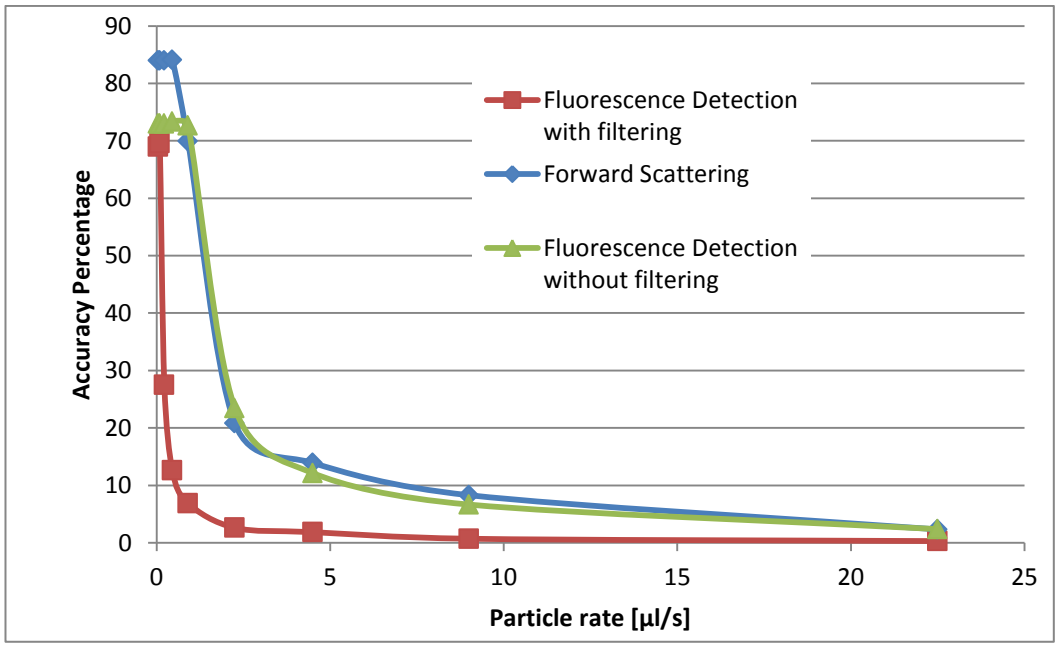

Figure 72: Percentage of Counting Accuracy for Fluorescent Particles as Forward Scattering and as Fluorescence Detection with and without Filtering

In Figure 72, the percentage of counting accuracy for the fluorescent particles when their forward scattering is counted is ~85% and it drops at 1µl/s. This counting accuracy is equal to the one obtained in section 4.5.2.1 for the forward

scatting of non-fluorescent particles. This figure also shows that the percentage of counting accuracy for fluorescent side detection without filtering is ~75% and drops 1µl/s. However, this result is different from the result obtained in section 4.5.2.2 when the counting accuracy was ~85% (but still drops at 1µl/s). This might be because there was extra noise in the lab coming from the AC mains or from the torch light which could be ON during this experiment. However, this result is still acceptable because it indicates that the counting accuracy when using the green filter (~70%) is lower than the counting accuracy without filtering (~75%). The increase in counted particles is due to the fact that some blue scattered light (not green fluorescent light) reached the side photo detector and was counted (when no filter was used).

Finally, the counting accuracy for the forward scattering of fluorescent particles is ~85% which is higher than the two cases when fluorescent scattering is detected with and without filtering (~70% and ~75%). This is because the forward scattered signals are stronger than the side scattered signals (fluorescent signals). Therefore the probability of detecting particles for the forward scattering is more than the probability of particles detection for the fluorescent scattering (side scattering).

4.7 Counting Accuracy of Fluorescence Particles Using APD and Normal Photodiode with and without Filtering

4.7.1 Design

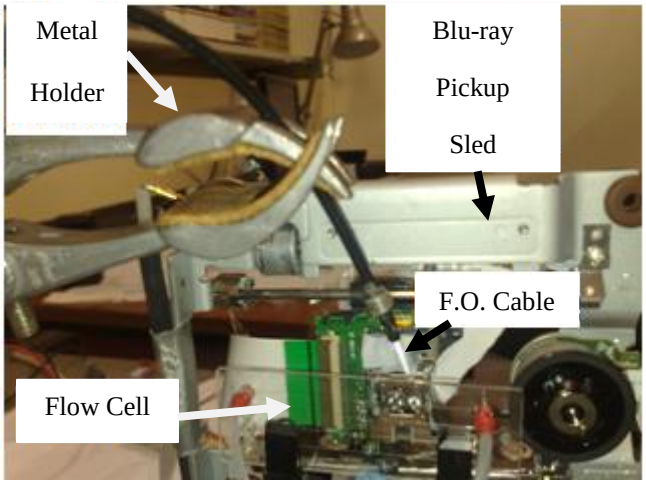

Figure 73: A picture of the Main Setup for APD Fluorescence Detection

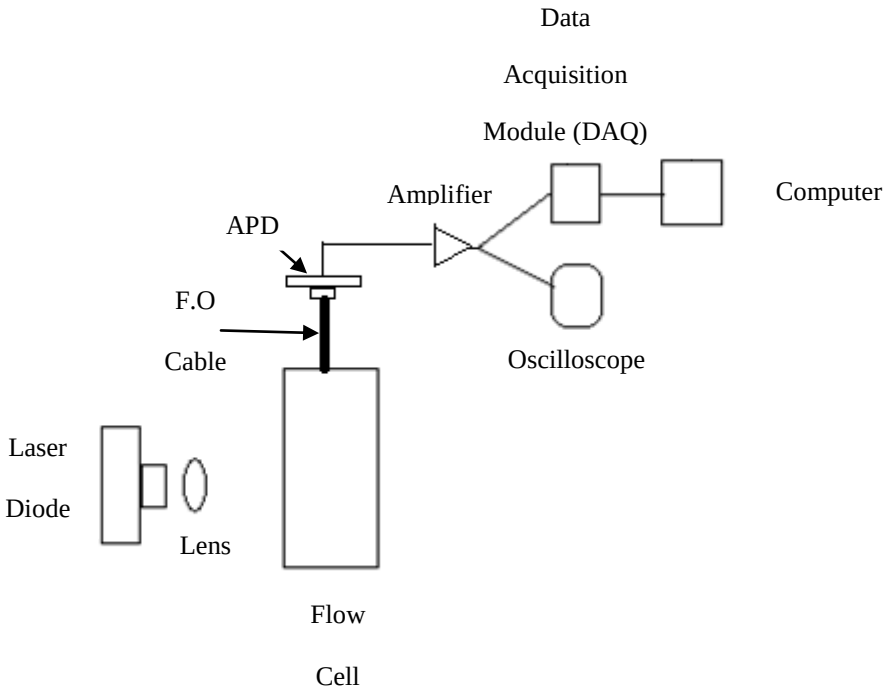

Figure 74: A diagram of the Main Setup for APD Fluorescence Detection

The percentage of counting accuracy for fluorescent particles is not high; for example it was ~%75 in the previous section (section 4.6.2). To increase the counting probability, an avalanche photodiode (APD) is used in this part for fluorescence detection. APD was used due to its high gain (40-100) and its better signal sensitivity. Figure 73 and Figure 74 show the experimental setup: the flow-cell ChipshopTM works as a waveguide, when fluorescence occurs, the waveguide carries the signal to the edge and it is collected by the F. O. (the F.O. cable is located at 90 degrees from the plane of the micro-fluidic chip). A matching index material was used between the F.O. cable and the flow cell to reduce any losses in the signal due to the difference in refractive index between air and glass. After that, the F.O. cable is connected to an APD which is connected to a voltage amplifier to amplify the fluorescent signals. After that, the signal is converted from analog to digital by the data acquisition module and then processed by a PC. The fluorescent particles used in this part are 9.9µm diameter, 1% solids, latex spherical beads and their category number is G1000B (Fluoro-Max^{TM}, Thermo Scientific).

4.7.2 Results and Discussion

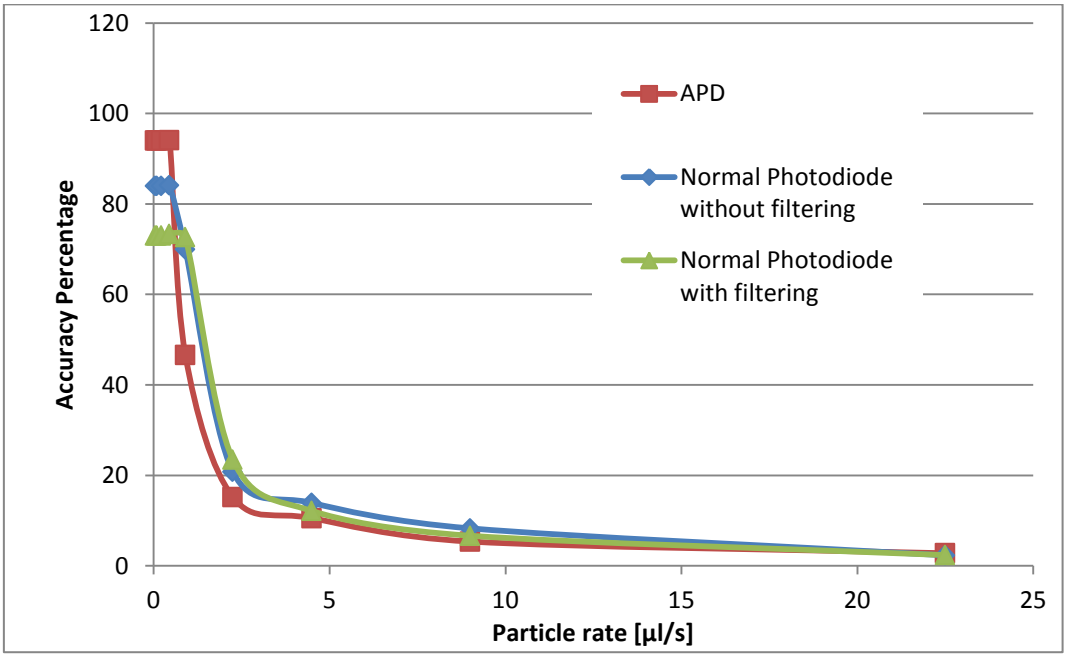

Figure 75: Percentage of Counting Accuracy of Fluorescent Particles Using APD and Normal Photodiode with and without Filtering

Figure 75, compares the percentage of counting accuracy for fluorescent particles using APD and normal photo diode with and without filtering. The percentage of counting accuracy with and without filtering is ~85% and ~75%, respectively and it drops at 1µm/s. These two results are better than the results obtained in the previous section (section 4.6.2) which were ~75% and ~70%, respectively. This might be because the AC mains and the torch were off and therefore no extra noise could be added to the Blu-ray cytometer which is too sensitive to light and noise. However, this result is expected because it indicates the counting accuracy when using the green filter (~75%) is lower than the counting accuracy without filtering (~85%). The increase in counting accuracy between these two cases is due to the fact that some blue scattered light reached the side photo detector and have been counted. Figure 75 also shows that the percentage of counting accuracy when using APD is very good (~95%) and it drops at 1µ/s. It is higher than the other two cases when using the normal photo diode with and without filtering (~75% and ~85%). This proves that the new setup (Figure 74) using the APD is a dramatic improvement to the counting accuracy (95%). However, Figure 74 shows that the rate at which counting accuracy drops is still the same (1µm/s) compared to the results taken from the old setup.

It should be noted that the highest rate was 10μm/s (see section 4.3.2) and this happened when the maximum particles rate was less than 5,000 particles/s. This rate dropped to 1μm/s (see section 4.5.2.2) when the maximum particles rate increased to about 50,000 particles/s. Therefore in order to have a high counting accuracy dropping rate, the examined particles rate should be less than 5,000 particles/s. Although the product of dropping rate and number of particles is constant (50,000) in this example, it is not constant for other measurements done for this project.

4.8 Counting Accuracy of 1μm Particles in Forward Scattering

4.8.1 Design

In this experiment, the aim was to check if the existing system can detect small particles, such as 1μm particles in diameter. According to Clow, Künnemeyer, Gaynor and Sharpe, polystyrene beads down to 3μm in diameter were successfully detected[14]. In their setup, a DVD was used for the detection of 3μm particles. Since the DVD they used has a larger spot focus (1.1 micron) than the spot focus of the Blu-ray (0.48 micron) used in this thesis, it was expected that the system used in this thesis was able to detect smaller particles.

The number of 1μm particles per volume was calculated in the same way described in section 4.5.2.1 for 10μm particles except that the diameter should be changed from 10μm to 1μm. The particles used in this part are 1μm diameter, 0.1% w/v, latex spherical beads and their category number is SL-010M (Latex Calibration Particles, ProSciTech).

4.8.2 Results and Discussion

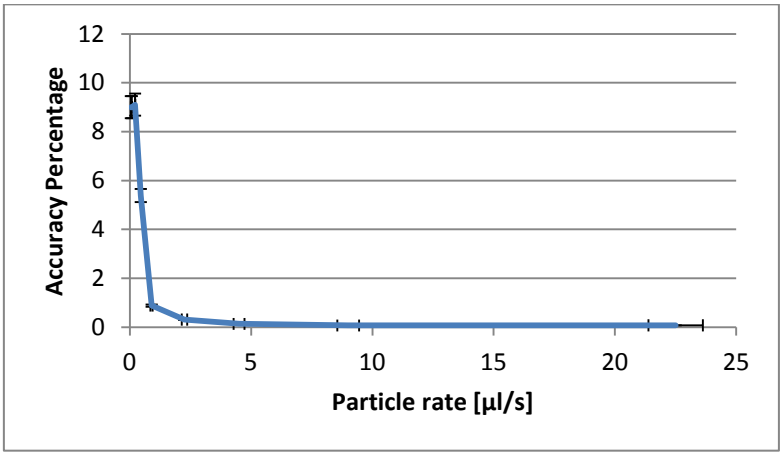

Figure 76: Percentage of Counting Accuracy of 1µm Particles

Figure 76 shows the percentage of counting accuracy for 1µm particles versus the flow rate of the system. This figure shows that the percentage of counting accuracy is very poor (~9%) and it drops at 1µm/s; whereas the counting accuracy for 20µm particles was ~90% (see section 4.4.2), the counting accuracy for 1µm diameter particles was only 9%. This low percentage of counting accuracy is expected due to the small size of examined particles and this indicates that the current system may not be able to detect nano particles.

4.9 Differentiation between 1µm and 10µm Particles

4.9.1 Design

After performing the last section (section 4.8), it was noticed that the cytometric output (the voltage recorded after particles scattering) is in the range of 0.0001 and 0.0009 for 1µm particles. However, the cytometric output for lager particles (for example 10µm particles) is in the range of 0.001 and 0.009. In this part, two different types of particles (1µm and 10µm) are mixed in one channel and their cytometric outputs detected by the photo detector were imported into an Excel™ Spreadsheet. The 1µm particles used in this part are 0.1% w/v, latex spherical beads and their category number is SL-010M (Latex Calibration Particles, ProSciTech). The 10µm particles used in this part are 0.1% w/v, latex spherical beads and their category number is SL10L (Latex Calibration Particles, ProSciTech).

4.9.2 Results and Discussion

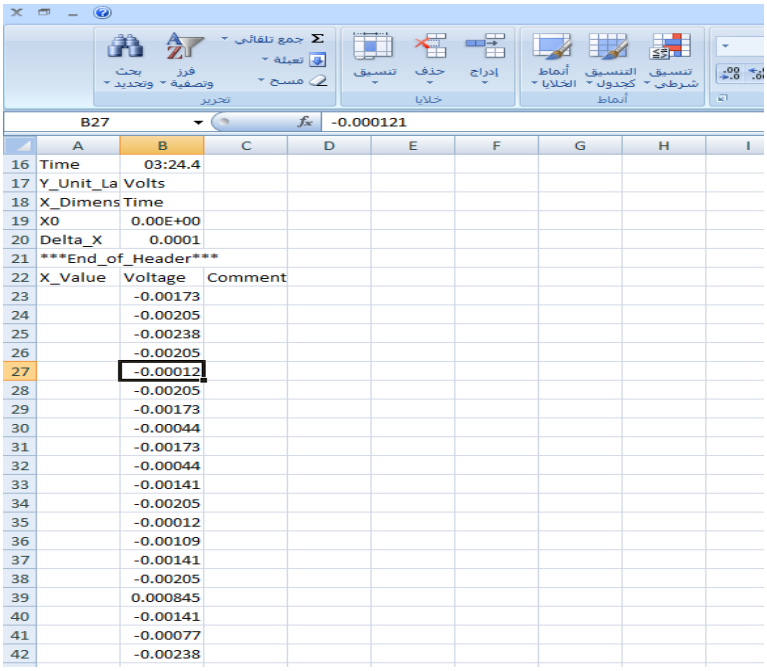

	A	B	C	D	E	F	G	H	I
16	Time	03:24.4							
17	Y_Unit_La	Volts							
18	X_Dimens	Time							
19	X0	0.00E+00							
20	Delta_X	0.0001							
21	***End_of_Header***								
22	X_Value	Voltage	Comment						
23		-0.00173							
24		-0.00205							
25		-0.00238							
26		-0.00205							
27		-0.00012							
28		-0.00205							
29		-0.00173							
30		-0.00044							
31		-0.00173							
32		-0.00044							
33		-0.00141							
34		-0.00205							
35		-0.00012							
36		-0.00109							
37		-0.00141							
38		-0.00205							
39		0.000845							
40		-0.00141							
41		-0.00077							
42		-0.00238							

Figure 77: The cytometric outputs for a mix of 1µm and 10µm Particles.

Figure 77 shows the cytometric outputs for a mix of 1µm and 10µm Particles. In this figure, there are 20 samples, 14 of them are in the range (0.001 and 0.009) and 6 of them are in the range (0.0001 and 0.0009). In this experiment, there were 2000, 1µm particles and 2000, 10µm particles in the channel (1:1 ratio). However, the ratio of 10µm to 1µm in Figure 77 is 7:3. The difference between the actual and experimental radio may be because the percentage of counting accuracy for 10µm particles is 80% whereas it is only 9% for 1µm particles. However, many analysis and experiments should be conducted in this part to reach to reliable results.

5. DISCUSSION

In this thesis, some important results have been achieved compared to other researchers in the same field. According to Clow, Künnemeyer, Gaynor and Sharpe, polystyrene beads down to 3μm in diameter were successfully detected[14]. However, in this thesis, 1μm latex spherical particles were detected but with poor counting accuracy. To illustrate this, whereas the counting accuracy for 20μm particles was ~90%, the counting accuracy for 1μm in diameter particles was only 9% which means that the current system may not be able to detect nano particles. The reason for the system used in this thesis to detect smaller particles than Clow, Künnemeyer, Gaynor and Sharpe's system is that this system uses Blu-ray with small spot focus while their system uses DVD with a larger spot focus. According to the reading done by the writer of this thesis, this system is the first system that uses Blu-ray (or even DVD) to count micro particles. For example, Yang, Hsiung, Hung, Chang, Liao and Lee have developed a counting system with a micro fabricated flow cytometer chip with counting accuracy of 98.5% (the error counting rate is 1.5%)[37]. Another example is the work done by Koch, Evans and Brunnschweiler[38]. They created a micro machined coulter counter system (it does not use DVD or Blu Ray) which is capable of detecting and counting 1.5μm and 0.5μm particles. However, these systems are better than the system used in this thesis in terms of counting accuracy, flow rate and particles sizes. Therefore, their systems can be used for medical applications, such as the quality control of high-tech fluids and the characterisation of biological cells. However, since our system is much cheaper than their system, it can be used in rivers to count the purity of water or in any other fields where accuracy is not very important and funds are limited.

There are some important notices from the experiments done for this report, such as personal vision and adjustment should not be fully trusted. This was taken when there was a big change in the counting accuracy for two different focusses though the difference in distance adjustmnt between the two focuses was very slight (0.05mm) and the position of the low counting accuracy focus was much better than the position of the high counting accuracy focus according to the human eyes but according to the data it was the other way around which means

that many focuses must be adjusted in order to take an optimal accounting accuracy.

Another considerable notice is that when mixing fluorescent and non-fluorescent particles, the counting accuracy decreases and the speed at which the accounting accuracy becomes poor is also decreases. This might be because the emissions of the fluorescent particles might hit other non-fluorescent particles, scatter and do not reach the detector.

Mie theory was also proven using the beam stop experiment since counting accuracy was poorer using a beam stop. This may be because the forward scattering is in the forward direction according to Mie theory and when a beam stop is installed in front of the laser beam it scatters light away from the detector. Other findings regarding the use of APD must be mentioned; the use of APD was very successful as a forward and side detector and the counting accuracy was dramatically improved after the use of APD.

It was checked that the system was able to detect fluorescent particle after the installation of a high bass filter which passes fluorescent wavelength signals (green) and blocks the blue ray signals. The counting accuracy without filtering was higher than the one with filtering which means than some blue scattered light (not green fluorescent light) reached the side photo detector and was counted (when no filter was used). Finally, it was found that this system is able to detect small size particles (1μm particles) and to distinguish between 1μm and 10μm particles though many analysis and experiments should be conducted in this part to reach to reliable results.

6. CONCLUSION

Flow cytometers have been used for the last 25 years and they are under a great deal of developments. Instead of the expensive types, new low cost cytometers have been developed that are based on CD, DVD and Blu-ray technologies. One of the main problems with these types is their weak detected signals which can be enhanced using phase contrast method or optical enhancements, such as an additional mirror to collect lost signals.

In this thesis, a low cost cytometer using a Blu-ray pickup was analysed and further developed. This includes the characterisation of the existing system and its performance and evaluation of count rate of the existing system for different flow rates and focus. Based on that, the best parameters for measurement conditions were determined. In order to get a percentage of counting accuracy up to 90%, the speed of 20μm particles should not exceed 10μl/s and the speed of 10μm particles should be less than 5μl/s. In both cases, the rate of particles should be less than 5,000 particles/s. Moreover, the system was set up for forward scatter as well as fluorescence; both were measured at the same time and it was found that both can be recorded and counted. In addition, it was checked that fluorescing particles can give a fluorescent count as well as scatter count. Furthermore, it was found that non-fluorescent particles can produce scatter count. The count rate for a mixture of fluorescent and non- fluorescent particles was also calculated and analysed.

The system was improved and progressed towards a setup of avalanche photodiode as detector for forward scattering as well as fluorescence. This development gave a very good counting percentage (95%). It was also checked that the system was able to detect fluorescent particle after the installation of a high bass filter which passes fluorescent wavelength signals (green) and blocks the blue ray signals. Finally, it was found that this system is able to detect small size particles, such as 1μm particles and to distinguish between 1μm and 10μm particles.

Some developments to this system can be done, including the use of voice coil motors (VCMs) as they can be used for alignment and focusing errors between the micro flow cell and optical pickup. Another improvement is the use of a laser noise reduction circuit to improve the weak signal-to-noise ratio (1:4) and to

improve detection sensitivity, particularly if back scatter signals are used. Finally, the detection sensitivity may also be improved by confining the particle flow within a sub-region of the channel cross-section. This can be achieved using a CO2 laser to mill double sided adhesive tape and working in co-ordination with the university glass blower.

7. APPENDIX

Laser Safety[39]

- The covers for the power supply and optical head should always be in place when a laser is energised. Built-in interlocks are designed to terminate laser emission when covers are removed. Under normal conditions, optical radiation will only be emitted through the output aperture. Removing the cover can lead to additional uncontrolled radiation output.
- Limit laser access to those individuals familiar with the equipment.
- Do not wear highly reflective jewellery, watches, etc. when working in the vicinity of a laser source.
- Try to keep all laser beams at heights far removed from normal eye level. In particular, when bending over (e.g. to pick up a dropped pen or pad), it is advisable to turn away from the laser apparatus and/or close your eyes as your head passes through "beam level."
- Do not operate high power lasers in the presence of flammables, combustibles, explosives, or volatile substances. Do not allow the beam to impinge upon flammable or combustible materials (e.g. wood, paper, paint, etc.).
- When the laser is on and the output beam is not being terminated in an experiment or optical system, the emitted light should be blocked. Use a laser power meter or some other non-reflecting, non-flammable object (i.e. a specially-designed 'beam dump').
- Always block the laser source when moving optical components into or out of the laser beam. In particular, do not place reflective objects into the optical path as the scattered light can be just as dangerous as the primary beam.
- Never look directly into either the main laser beam or any secondary/stray beam. Never look down a beam towards its source.
- Do not expose skin to direct laser emission as its intensity can be sufficient to cause severe flesh wounds.
- When aligning optical components, it is advisable to reduce the output power of the laser to as low a level as possible. This minimises the danger associated with stray reflections or refractions.

- Warning signs are required and access to the laser area must be limited whenever certain high power lasers are in operation. When initiating laser emission, ensure you inform all other individuals in the room.
- Whenever possible, wear the appropriate laser safety goggles. There are two hazards that exist when wearing such devices while operating lasers. First, the glasses make the laser beam itself invisible, thereby increasing the danger of inadvertent skin burns. Second, laser goggles may not afford sufficient protection if a very powerful laser beam is viewed directly.

8. REFERENCES

1. A. Yen, *Flow cytometry: Advanced research and clinical applications*, USA, CRC Press, 1989.
2. M.G. Ormerod, *Flow cytometry: A practical approach*, UK, Oxford University Press, 2000.
3. M. R. Melamed, T. Lindmo, M. L. Mendelsohn, *Flow cytometry and sorting*, USA, Wiley-Liss, 1990.
4. Yong, H.; Ning, C.; Borninski, J.; Rubinsky, B. In *A novel microfluidic cell-chip for single cell analysis and manipulation*, Proceedings IEEE Sixteenth Annual International Conference on Micro Electro Mechanical Systems, pp 403-6, 19-23 Jan. 2003, Piscataway, NJ, USA, IEEE: Piscataway, NJ, USA, 2003.
5. Cho, Y. H.; Yamamoto, T.; Sakai, Y.; Fujii, T.; Beomjoon, K., Development of microfluidic device for electrical/physical characterization of single cell. *Journal of Microelectromechanical Systems,* **,** *15* (2), 287-95, 2006.
6. H. M. Shapiro, *Practical flow cytometry*, USA, Wiley-Liss, 1995.
7. T. Vo-Dinh, *Biomedical photonics handbook*, USA, CRC Press, 2003.
8. Cytometer main components. http://www.abcam.com/ps/CMS/Images/Flow-Cytometry-diagram2.jpg (accessed 12 Jan 2012).
9. A commercial flow Cytometer manufactured by iCyt. http://industrial.productwiki.com/icyt-eclipse-flow-cytometry-analyzer/ (accessed 17 Feb 2012).
10. A commercial cell sorter manufactured by Becton Dickinson. http://www.csm.bio.dtu.dk/Instrument%20Center/Resources/Flow%20Cytometer%20and%20Cell%20Sorter.aspx (accessed 17 Feb 2012).
11. Kyung-Ho, K.; Seung-Yop, L.; Sookyung, K.; Seung-Hwan, L.; Seong-Gab, J., A new DNA chip detection mechanism using optical pick-up actuators. *Microsystem Technologies, 13* (8-10), 1359-69, 2007**.**
12. Kostner, S.; Vellekoop, M. J., Low cost cytometer based on a Dvd pickup head. In *Eleventh International Conference on Miniaturized Systems for Chemistry and Life Sciences*, Paris, FRANCE, pp 739-741, 2007,
13. Kostner, S.; Vellekoop, M. J., DVD pickup heads for optical measurement applications. *Elektrotechnik und Informationstechnik***,** *125* (3), 98-101, 2008**.**
14. A Clow, R. Kunnemeyer, P. Gaynor, J. Sharpe, "Low cost optical particle detection for Lab on Chip systems based on DVD technology", *The International Society for Optical Engineering (SPIE)* 6799, 67990S1-9, December ,2008.
15. Kefauver, A. P.; Patschke, D., *Fundamentals of digital audio*. New ed.; A-R Editions Inc.: Middleton, Wis., Vol. v. 22, p xiv, 190, 2007.
16. DVD Optical Pickup Head Setup. http://www.nitto-optical.co.jp/english/feature/pickup.html (accessed 12 Jan 2012).
17. PHR-803T Pickup and Dismantled View. http://c4r0.skrzynka.org/_hv/lasers/405_41_big.jpg (accessed 13 Jan 2012).
18. Toshiba Announces Discontinuation of HD DVD Businesses. http://www.toshiba.co.jp/about/press/2008_02/pr1903.htm (accessed 17 Feb 2012).
19. Latest Semiconductor Diodes in Cytometry. http://www.asiatoday.com.au/feature_reports.php?id=498 (accessed 12 Jan 2012).
20. J. V. Watson, *Introduction to flow cytometry*, Cambridge, Cambridge University Press, 1991.
21. Solomon, C.; Breckon, T., *Fundamentals of digital image processing : A practical approach with examples in Matlab*. Wiley-Blackwell: Chichester, West Sussex ;Hoboken, NJ, p xiv, 328, 2011.

22. Forward Scatter Histogram. http://www.biology.sjsu.edu/specialprogs/flocyto/html/paintut.html (accessed 13 Jan 2012).
23. Ramm, A. G., *Wave scattering by small bodies of arbitrary shapes*. World Scientific: Singapore ; Hackensack, NJ, p xviii, 293, 2005.
24. Rayleigh Scattering. http://hyperphysics.phy-astr.gsu.edu/hbase/atmos/blusky.html (accessed 17 Feb 2012).
25. Sharkov, E. A., *Breaking ocean waves :Geometry, structure and remote sensing*. Springer: Berlin ; New York, p xxii, 278, 2007.
26. 2D Scatter Plot of Blood. http://www.anesthesia-analgesia.org/content/90/1/206.full(accessed 17 Feb 2012).
27. Energy State Diagram for Fluorescence. http://scienceblogs.com/purepedantry/2007/11/two_photon.php (accessed 13 Jan 2012).
28. Rendell, D.; Mowthorpe, D. J., *Fluorescence and phosphorescence spectroscopy*. Published on behalf of ACOL London by Wiley: Chichester West Sussex ;New York, p xix, 419, 1987.
29. Two Colour Experiment. http://www.invitrogen.com/site/us/en/home/References/Molecular-Probes-The-Handbook/Fluorophores-and-Their-Amine-Reactive-Derivatives/Alexa-Fluor-Dyes-Spanning-the-Visible-and-Infrared-Spectrum.html (accessed 13 Jan 2012).
30. Two Colour Dot Plot. http://www.antibodiesonline.com/resources/17/607/Flow+cytometry+FACS+Principle+and+experimental+setup/ (accessed 13 Jan 2012).
31. Rahman, M., Introduction to Flow Cytometry. http://static.uk-plc.net/library/abd/uploads/Flow-Cytometry.pdf. (accessed 13 Jan 2012).
32. De Graef, M., *Introduction to conventional transmission electron microscopy*. Cambridge University Press: Cambridge, U.K. ;New York, N.Y., p xxi, 718, 2003.
33. Phase Contrast Method. http://www.microscopyu.com/tutorials/java/phasedicmorph/(accessed 13 Jan 2012).
34. Bertein, J.-C.; Ceschi, R., *Discrete stochastic processes and optimal filtering*. ISTE USA: Newport Beach, CA, p ix, 287, 2007.
35. A Clow, 2011, *Low Cost Cytometry Using a Blu-ray Pickup*, internal report 2011, University of Waikato, Hamilton.
36. Kendall, M. G.; Stuart, A.; Ord, J. K., *Kendall's advanced theory of statistics*. 5th ed / ed.; Griffin: London, p xvi, 604, 1987.
37. Sung-Yi, Y.; Suz-Kai, H.; Yung-Ching, H.; Chen-Min, C.; Teh-Lu, L.; Gwo-Bin, L., A cell counting/sorting system incorporated with a microfabricated flow cytometer chip. *Measurement Science & Technology***,** *17* (7), 2001-9, 2006**.**
38. Koch, M.; Evans, A. G. R.; Brunnschweiler, A., Design and fabrication of a micromachined Coulter counter. *Journal of Micromechanics and Microengineering***,** *9* (2), 159-61, 1999**.**
39. School of Science and Engineering, *Laser Safety Policy*, University of Waikato, Hamilton, NZ, 2008.